Materials Today Communications 57 (2026) 116582

Contents lists available at ScienceDirect

Materials Today Communications

journal homepage: www.elsevier.com/locate/mtcomm

High temperature tribology of additively manufactured titanium alloys: A condition dependent review

Mehmet Can Katmer [a,b], Onur Cavusoglu [c,*], Hakan Gürün [c], Ömer Asal [c]

[a] Anova R&D Technologies Industry and Trade Inc. Co, Ankara, 06510, Türkiye
[b] Gazi University, Graduate School of Natural and Applied Sciences, Department of Manufacturing Engineering, Ankara 06560, Türkiye
[c] Gazi University, Faculty of Technology, Department of Manufacturing Engineering, Ankara, 06560, Türkiye

ARTICLE INFO

Keywords:
Additive manufacturing
Titanium alloys
High-temperature tribology
Wear mechanisms
Tribo-layers
Specific wear rate

ABSTRACT

Additively manufactured (AM) titanium alloys are increasingly considered for sliding components at elevated temperature, but published wear data are difficult to compare because test conditions differ widely. This review compiles dry sliding data from 20 elevated-temperature studies, identified following a PRISMA-informed procedure, and 13 room-temperature studies on L-PBF, EB-PBF, DED and WAAM material of commercially pure titanium, Ti-6Al-4V, near-α, β and γ-TiAl alloys, and compares them within each study after stratification by counterface and contact geometry. AM materials reached wear rates within about a factor of two of conventionally processed material, and room-temperature hardness did not consistently rank wear resistance. With increasing temperature, the specific wear rate increased, decreased or changed non-monotonically depending on counterface, contact configuration and load, while friction did not follow wear. TiO_2 was the oxide most consistently identified in tribo-layers by phase analysis, and the presence of a tribo-layer did not consistently coincide with lower wear. Reported wear mechanisms did not follow fixed temperature boundaries. Recommendations for reporting test conditions, characterizing tribo-layers and measuring hot hardness are given.

1. Introduction

Additively manufactured titanium alloys –encompassing commercially pure, (α+β), near-α, metastable β and γ-TiAl intermetallic systems– are widely used in high-performance sectors, including aerospace, defense, and biomedical engineering, owing to their high specific strength, design flexibility, corrosion resistance, and biocompatibility [1–6]. In the biomedical field, AM enables custom-tailored orthopedic implants, dental prostheses and cranial/maxillofacial reconstructions [2,4,7]. In the automotive sector, titanium alloys are established for lightweight engine and chassis components such as valves, connecting rods and suspension springs [8,9], and AM is increasingly explored for lightweight, geometrically complex variants of such parts [10]. Furthermore, additive manufacturing (AM) facilitates the direct fabrication of conformal cooling channels for injection molding as well as complex 3D lattice and open-cellular architectures, thereby yielding lightweight structures with favorable energy absorption and mechanical properties for demanding load-bearing applications [11,12].

Presently, Powder Bed Fusion (PBF) techniques –including Laser Powder Bed Fusion (L-PBF, also referred to as SLM) and Electron Beam Powder Bed Fusion (EB-PBF, also referred to as EBM; the term EB-PBF is used throughout this review)– are predominantly used due to their high resolution [4,11,13,14], while Directed Energy Deposition (DED), including its wire-arc variant (WAAM), is increasingly preferred for large-scale, near-net-shape manufacturing and localized component repair [15–18]. However, the layered nature of these PBF and DED processes gives rise to intricate thermal histories, characterized by rapid solidification and recurrent heating and cooling cycles [19]. Consequently, the resulting microstructure of AM titanium alloys differs significantly from their wrought counterparts and varies depending on the energy source and processing route used [5]. In L-PBF, the high cooling rates (10^3–10^8 K/s) produce a fine, acicular martensitic (α′) structure within columnar prior-β grains [6,20–22]. Conversely, EB-PBF has been shown to favor the development of a coarser, near-equilibrium lamellar α + β microstructure when operated at higher bed temperatures (~600 °C–700 °C) due to *in-situ* thermal annealing [6,23]. These microstructural features directly influence mechanical properties, particularly hardness, which enters the classical Archard wear equation as the material property that controls the wear volume per unit load and sliding distance [24]. However, the hardness relevant to Archard's relation is that of the near-surface material during sliding; at elevated

* Corresponding author.
E-mail address: onurcavusoglu@gazi.edu.tr (O. Cavusoglu).

https://doi.org/10.1016/j.mtcomm.2026.116582
Received 18 September 2026; Received in revised form 27 October 2026; Accepted 3 November 2026
Available online 5 November 2026
2352-4928/© 2026 The Author(s). Published by Elsevier Ltd. This is an open access article under the CC BY license (http://creativecommons.org/licenses/by/4.0/).

Nomenclature

a	Radius of the Hertzian contact (m)
E	Elastic Modulus (GPa)
E^*	Effective elastic modulus of the contact (GPa)
F	Normal load (N)
p_0	Initial maximum Hertzian contact pressure (MPa)
R	Ball radius (m)
S	Sliding Distance (m)
T	Testing Temperature (°C)
v	Sliding Velocity (m/s)
V	Wear volume (mm^3)
α	Alpha phase
α′	Martensitic alpha prime phase
β	Beta phase
ν	Poisson's ratio
Al_2O_3	Aluminum Oxide
AM	Additive Manufacturing
CoF	Coefficient of Friction
CP-Ti	Commercially Pure Titanium
DED	Directed Energy Deposition
DMLS	Direct Metal Laser Sintering
EB-PBF	Electron Beam Powder Bed Fusion
EBM	Electron Beam Melting
EDS	Energy Dispersive X-ray Spectroscopy
HV	Vickers Hardness
L-DED	Laser Directed Energy Deposition
L-PBF	Laser Powder Bed Fusion (Note: Often interchangeable with SLM)
LENS	Laser Engineered Net Shaping
PRISMA	Preferred Reporting Items for Systematic Reviews and Meta-Analyses
SEM	Scanning Electron Microscopy
SLM	Selective Laser Melting
SWR	Specific Wear Rate (mm^3/(N·m))
TEM	Transmission Electron Microscopy
Ti-64	Ti-6Al-4V alloy (used in figure legends)
TiO_2	Titanium Dioxide
WAAM	Wire Arc Additive Manufacturing
WC–Co	Tungsten Carbide–Cobalt
XPS	X-ray Photoelectron Spectroscopy
XRD	X-ray Diffraction

temperatures this is governed by hot hardness, flow stress, strain-hardening capability and dynamic thermal softening, and is further modified by tribologically transformed layers and tribo-oxides, rather than by the room-temperature bulk hardness usually reported for AM alloys [25–28]. While the tribological behavior of AM titanium alloys at room temperature has been the subject of considerable research, their performance under aggressive operating conditions, particularly at elevated temperatures, remains a significant challenge [7,29,30]. In aero-engine compressors and high-temperature structural assemblies, where titanium alloys are used close to their upper service temperatures, components are exposed to concurrent thermal stress and sliding or fretting contact, underscoring the necessity for a comprehensive understanding of temperature-dependent wear mechanisms, including the formation and breakdown of tribo-layers and the thermal softening of the matrix [18,27,28].

Despite a growing number of studies, the elevated-temperature tribology of AM titanium alloys remains difficult to generalize. The available high-temperature data were obtained with ball-on-flat, ball-on-disc, pin-on-disc and ring-on-disc configurations, against counterfaces ranging from Al_2O_3, Si_3N_4, SiC and WC–Co to bearing and maraging steels and an Fe–Ni-based superalloy, under normal loads of 2–200 N, sliding speeds of 0.006–2 m/s, sliding distances of 3.6–2000 m and temperatures up to 1000 °C [18,27,28,31–45]. Within single studies, the temperature at which wear peaks, and even whether a peak exists, changes with the contact load [35,39] and with the test duration [28], and in a test in high vacuum, where tribo-oxidation is suppressed, wear increased by more than an order of magnitude between room temperature and 850 °C [40]. Wear is, moreover, reported in different metrics (wear volume, wear depth, mass loss or wear per unit sliding distance) [32,34,41,46], and the tribo-oxides invoked to explain mild wear are frequently inferred from elemental (EDS) maps rather than identified by phase-sensitive techniques [27,31,35,36,39,45]. The oxide-rich tribo-layers and the tribologically transformed, nanocrystalline subsurface layers that develop beneath them during sliding are central to the interpretation of elevated-temperature wear [18,27,28,37]; their formation and breakdown depend on the contact load [39], the sliding time [28] and the counterface [37]. Consequently, reported transition temperatures are strongly condition-dependent and cannot be transferred directly between studies. Existing reviews on the tribology of AM metals and titanium alloys focus mainly on room-temperature behavior and processing effects [15,19,25,26,30,47] and, to the authors' knowledge, none has compiled the elevated-temperature data for AM titanium alloys in a systematic and condition-stratified manner. The factors considered in this review –AM processes, post-processing, microstructure, mechanical properties and wear mechanisms, together with the main fields of application– are shown schematically in Fig. 1.

Accordingly, the objective of this review is not to propose a single, universal sequence of transition temperatures, but to establish a condition-dependent framework for interpreting the elevated-temperature wear of AM titanium alloys. To this end, (i) the elevated-temperature literature was identified and screened following a PRISMA-informed procedure, whereas the room-temperature benchmark was compiled using a defined selection rule (Section 2) [48]; (ii) wear data were extracted from the original sources, converted to a common specific wear rate (SWR, mm^3/(N·m)) wherever the reported quantities allowed it, and analyzed within each study after stratification by counterface, contact geometry and test conditions; (iii) ball-contact tests were characterized by their initial Hertzian contact pressure, calculated uniformly for all studies, and the complete test conditions are provided as supplementary data; and (iv) tribochemical interpretations were graded according to whether oxide phases were directly identified (XRD, Raman spectroscopy, XPS) or only inferred. Section 3 summarizes the process-dependent microstructures of AM titanium alloys. Section 4 analyzes their room- and elevated-temperature wear and friction behavior, the role of hardness, the effects of load and test duration at constant temperature, and the formation and stability of tribo-layers, and compiles the author-reported wear mechanisms as a function of temperature, distinguishing directly identified from inferred tribo-oxides. The conclusions and an outlook on the remaining evidence gaps follow.

2. Review methodology

The elevated-temperature literature was compiled with a structured search and screening procedure informed by the PRISMA 2020 statement [48] (Section 2.1). Room-temperature dry sliding of AM titanium alloys has been studied far more extensively, and an exhaustive survey was outside the scope of this review; room-temperature data were therefore used only as a benchmark, compiled with a defined selection rule: dry sliding studies of monolithic AM titanium alloys reporting a specific wear rate, or the quantities needed to calculate it, chosen to cover each AM route, each alloy class and the main post-processing

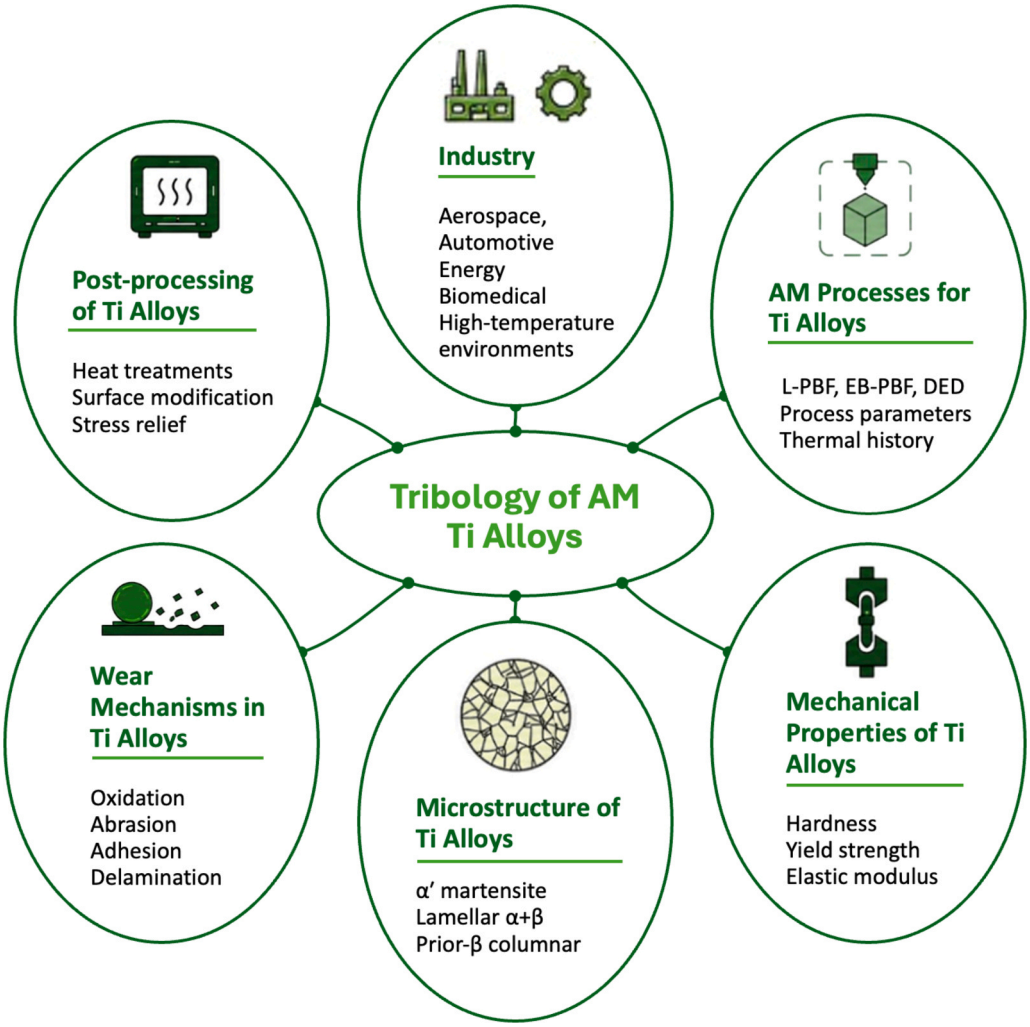


Fig. 1. Schematic overview of the topics addressed in this review of the tribology of AM titanium alloys: fields of application, AM processes, post-processing, microstructure, mechanical properties and wear mechanisms.

variables [17,32,49–59], complemented by the room-temperature baselines of the elevated-temperature studies. Two studies that report only percentage changes relative to the as-built condition [57,58] were retained for qualitative comparison. Tribocorrosion tests were excluded. The search strings, screened records, extracted data and calculations are provided as supplementary material (Tables S1–S4).

2.1. Search strategy and study selection

Scopus and the Web of Science Core Collection were searched on 21 October 2026 for English-language articles and reviews published since 2010, combining terms for the AM process, the titanium alloy, elevated temperature and sliding wear (Table S3); the database search was complemented by forward citation searching of three key studies [37, 39,60]. Studies were included if they tested a monolithic AM titanium alloy or titanium aluminide (composites only with a monolithic control tested under identical conditions) in dry sliding, at least one test temperature was above room temperature, and a wear quantity was reported together with the normal load. Excluded were studies outside this material scope (E1), on coatings, claddings or surface treatments (E2), on composites without a monolithic control (E3), with room-temperature tests only (E4), reviews (E5), lubricated or tribocorrosion tests (E6) and other test types (E7). The selection process is shown in Fig. 2: of 241 records (166 after removal of duplicates), 20 elevated-temperature studies were included [18,27,28,31–46,61]. Sixteen report specific wear rates at two or more temperatures and form the quantitative synthesis; four provide only wear depths [32,34], mass-loss ratios [46] or a single test temperature [61] and are used qualitatively. Tests in high vacuum [40] and small-amplitude (±150 μm) reciprocating tests [18] were kept as separate strata.

2.2. Data extraction and normalization

Test conditions, material data, wear and friction results and the worn-surface characterization techniques were extracted for each study (Table S1), from the text or tables where possible and otherwise by digitizing the published figures. Wear was expressed as the specific wear rate, SWR = V/(F·S) (mm^3/(N·m)), where V is the wear volume, F the normal load and S the sliding distance; mass losses were converted to volumes with the alloy density, and the sliding distance of reciprocating tests was calculated from stroke, frequency and duration when not stated. Data extraction was assisted by an AI tool (Claude, Anthropic); all extracted values, reported wear mechanisms and tribo-layer findings were checked by the authors against the original publications.

Absolute wear rates measured in different laboratories differ by more than an order of magnitude even for the same alloy, because they depend on the counterface, contact geometry and test rig. Effects of temperature, load, sliding time and manufacturing method were therefore evaluated within each study, and the data were grouped by manufacturing method, counterface class, contact geometry and

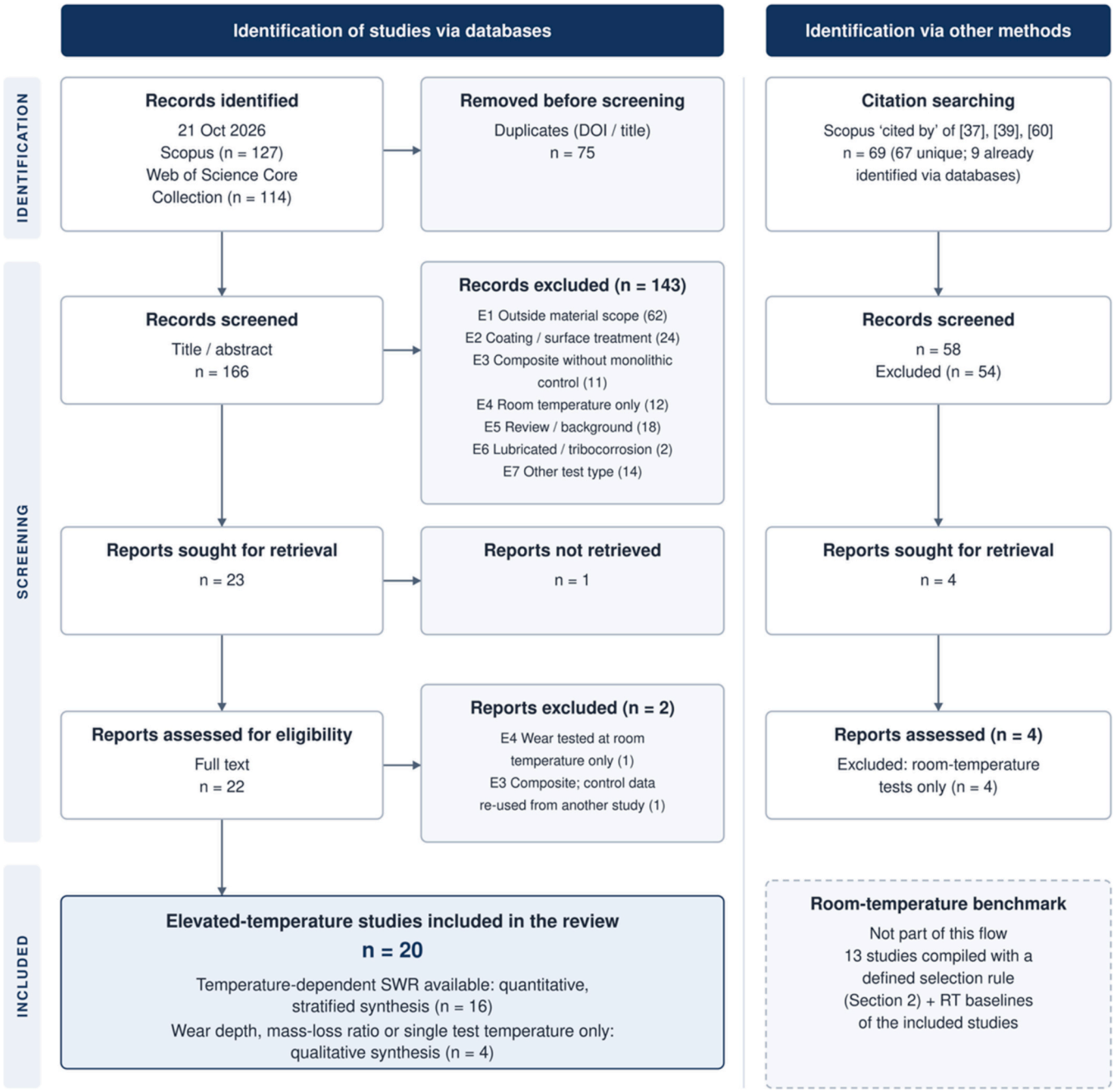


Fig. 2. PRISMA 2020 flow diagram of the identification, screening and inclusion of elevated-temperature studies. The room-temperature benchmark was compiled separately with a defined selection rule.

environment for presentation. Load and sliding-time effects were evaluated only in studies that varied them at several temperatures [27,28,35,39,44]. Two studies were used for within-study trends only: in one, the reported specific wear rates are several times higher than those estimated from the wear depths and test parameters given in the same study [39]; in the other, they are about four orders of magnitude lower than in all other studies, which may indicate a unit inconsistency that could not be verified [42]. Two statistical analyses were performed (Table S4). The relation between normal load and temperature sensitivity was assessed with Spearman's rank correlation using one value per study, the ratio of the specific wear rates at the highest and the lowest test temperature (geometric mean over the test series of the study). The reported mechanisms were classified with decision trees, a random forest and multinomial logistic regression (scikit-learn), using only the points for which the authors stated a dominant mechanism; the accuracy was determined by leave-one-study-out validation, in which each study was predicted by a model trained on the remaining studies.

2.3. Initial contact pressure

For ball-on-flat and ball-on-disc tests, the initial maximum Hertzian contact pressure p_0 was calculated uniformly from the normal load F, the ball radius R and the elastic constants of the specimen and counterface (E_i, ν_i; Table S2) [62]:

$$E^* = \left[\frac{1-\nu_1^2}{E_1} + \frac{1-\nu_2^2}{E_2}\right]^{-1}, a = \left(\frac{3FR}{4E^*}\right)^{\frac{1}{3}}, p_0 = \frac{3F}{2\pi a^2} \quad (1)$$

The resulting values range from 560 to 2829 MPa. Since p_0 is the

initial elastic pressure, falls as the wear scar grows and in several tests exceeds the onset of yielding ($p_0 \approx 1.6$ times the yield strength [62]), it is used only as an index of initial contact severity. Elastic constants were taken from the included studies where reported [18,31] and otherwise from handbook data or published measurements (e.g., E = 113.8 GPa and $\nu = 0.342$ for Ti-6Al-4V [63]; WC–Co [64]; SiC [65]); because the compliance of the titanium specimen dominates E*, a ± 20% change in the counterface modulus alters p_0 by less than 6%. All quantities were calculated in SI units (N, m, Pa), and p_0 is reported in MPa. Room-temperature values were used at all temperatures; even a 20% lower modulus of the titanium alloy at 500–600 °C would reduce p_0 by only about 10%.

2.4. Wear mechanisms and tribo-layer evidence

The wear mechanisms reported at each test temperature were assigned to four classes: abrasive (including three-body abrasion and ploughing), adhesive (including material transfer), oxidative, or delamination/fatigue. A mechanism was recorded as dominant only where the authors explicitly ranked it above the others or named it as the only mechanism; where mechanisms were named without such a ranking, the point was recorded as mixed (Table S4). One study [39] was not used for this purpose because its mechanism assignments are inconsistent between text and figures. Claims of oxide tribo-layers were classified by the supporting evidence: oxide phases identified on the worn surface by XRD or Raman spectroscopy, oxidation states determined by XPS, oxygen enrichment detected by EDS only, or SEM observation without chemical analysis.

3. Microstructural characteristics of AM titanium alloys

The tribological performance of additively manufactured titanium alloys is strongly influenced by process-induced microstructural features, particularly phase composition, grain morphology, and defect distribution [22,66]. In additively manufactured (AM) materials, these features are dictated by process-specific thermal histories involving rapid solidification and cyclic reheating, resulting in significant deviations from conventional wrought or cast microstructures [22,66,67]. These variations directly influence hardness, plastic deformation behavior, and the mechanical stability of tribo-layers, and thus set the initial conditions for room- and elevated-temperature wear [22,68]. The comparison below focuses on the benchmark alloy Ti-6Al-4V [22,67], for which most tribological data exist; commercially pure titanium (CP-Ti) [30,69,70], near-α alloys (Ti-6242, TA15, TC11) [18,31,46], metastable β alloys (Ti-Nb, TNTZ) [66,68,71] and γ-TiAl [32,56] are addressed where data are available.

3.1. Laser powder bed fusion (L-PBF)

The L-PBF process, which encompasses Selective Laser Melting (SLM) and Direct Metal Laser Sintering (DMLS), involves extremely rapid solidification rates (10^3–10^8 K/s) and steep thermal gradients [13,22]. This rapid cooling process effectively suppresses the diffusion-controlled transformation of the high-temperature β phase into the equilibrium α phase. Instead, a diffusionless transformation occurs, resulting in a non-equilibrium acicular martensitic structure (α′ or α″) [30,66,70].

3.1.1. Morphology

The microstructure of as-built L-PBF Ti-6Al-4V is characterized by fine, needle-shaped α′ martensite laths hierarchically arranged within prior-β columnar grains [20,66,67]. These prior-β grains exhibit epitaxial growth along the build direction (*Z*-axis) due to maximum heat extraction toward the substrate [30,66]. In metastable β titanium alloys, this rapid thermal cycling can retain a monolithic β matrix containing dense dislocation networks, cellular sub-structures, and localized micro-segregation [66,68].

3.1.2. Mechanical implication

The fine martensitic structure yields high tensile strength and hardness in as-built L-PBF Ti-6Al-4V (about 370–430 HV in the included studies) compared with wrought material (about 320–330 HV) [28,33,35,36]. The epitaxial growth of prior-β grains induces microstructural anisotropy [30,67], although its effect on sliding wear has been found to be small for EB-PBF material [31]. The high hardness is frequently accompanied by limited ductility, high tensile residual stress and susceptibility to micro-cracking, which can promote brittle fracture of surface asperities during initial sliding contact [21,70,72,73]. Nevertheless, the wear rates of L-PBF, EB-PBF and wrought Ti-6Al-4V measured under identical conditions are often similar despite hardness differences of up to about 100 HV [35,50], indicating that room-temperature hardness alone does not rank their wear resistance.

3.2. Electron beam powder bed fusion (EB-PBF)

Conversely, the EB-PBF process occurs within a high-vacuum chamber that is maintained at an elevated preheating temperature (~600 – 700 °C) to mitigate thermal gradients [6,23]. This elevated bed temperature functions as an *in-situ* thermal annealing and stress-relief mechanism during fabrication [23].

3.2.1. Morphology

Lower local cooling rates permit diffusion-driven atomic transport, suppressing the retention of metastable acicular martensite (α′) [74,75]. The resulting microstructure is characterized by a fine Widmanstätten (α+β) basketweave morphology or lamellar α colonies situated within prior-β grains [23,67,74]. When processing advanced β-type systems via EB-PBF, such as *in-situ* silicide-reinforced Ti-35Nb-5Ta-7Zr-xSi (TNTZ-Si), the thermal environment promotes uniform precipitation of submicron $(Ti, Zr)_3Si$ silicides within equiaxed and elongated β grains [71].

3.2.2. Mechanical implication

Consequently, as-built EB-PBF Ti-6Al-4V parts exhibit moderate hardness (~330–370 HV) compared to L-PBF parts but offer superior ductility [67,76]. This microstructural state is less prone to brittle asperity fracture and subsurface delamination; its lower hardness may favor adhesion and material transfer, although the measured wear rates of EB-PBF and L-PBF Ti-6Al-4V are similar [35,50].

3.3. Directed energy deposition (DED)

DED techniques –encompassing Laser Metal Deposition (LMD), Laser Engineered Net Shaping (LENS), and Wire Arc Additive Manufacturing (WAAM)– involve the continuous feeding of powder or wire into a melt pool created by a focused energy source. DED is well suited to large near-net-shape parts and to localized component repair [15,16].

3.3.1. Morphology

The cooling rates in DED (10^2–10^4 K/s) are generally lower than those in L-PBF [16,22]. The microstructure frequently gives rise to a combination of fine basketweave α lamellae and retained β, although martensitic α′ can form in the uppermost finishing layers where cooling occurs most rapidly. In WAAM, the higher heat input of the arc produces coarse prior-β grains with a lamellar or basketweave α + β structure; reported hardness values are about 340–420 HV for Ti-6Al-4V and TA15 [17,18]. In intermetallic systems such as DED-fabricated γ-TiAl alloys, rapid layerwise thermal cycles promote alternating lamellar ($\alpha_2 + \gamma$) colonies with localized β_0/B2 phase segregation [3,15].

3.3.2. Mechanical implication

DED parts generally exhibit mechanical properties that fall between

those of L-PBF and EB-PBF. However, the process is susceptible to defects, including incomplete fusion, which can act as sites for crack initiation. Furthermore, these defects facilitate the detachment of unmelted particles during sliding, leading to third-body abrasion [16,77].

3.4. Summary of microstructural differences

The disparate thermal histories of these AM processes result in variations in phase composition, grain size, and hardness, which define the initial state of the sliding contact; as discussed in Section 4, hardness alone is not a reliable indicator of wear resistance. A comparison of these characteristics for the benchmark Ti-6Al-4V alloy, complemented by WAAM, is presented in Table 1.

The corresponding morphologies are illustrated in Fig. 3: the transition from rapid cooling in L-PBF to the near-equilibrium conditions of EB-PBF and the layerwise re-melting of DED results in progressive microstructural coarsening and phase redistribution.

4. Tribological behavior at room and elevated temperature

The wear of AM titanium alloys results from the competition between the mechanical removal of material, the formation and breakdown of tribo-layers, and the temperature-dependent strength of the near-surface material [26,29,47]. This section first summarizes the room-temperature benchmark (Section 4.1) and then analyzes the effects of temperature on wear (Section 4.2) and friction (Section 4.3), the effects of load and test duration at constant temperature (Section 4.4), the tribo-layers and the role of hardness (Section 4.5), before compiling the wear mechanisms reported at each test temperature (Section 4.6).

4.1. Room-temperature benchmark

Table 2 summarizes the room-temperature dry sliding data of the benchmark set defined in Section 2. Apart from two studies discussed separately below [49,54], the specific wear rates span more than an order of magnitude, from about 0.4×10^{-4} mm^3/(N·m) for L-PBF commercially pure titanium against a hard-faced steel disc [55] to about 16×10^{-4} mm^3/(N·m) for WAAM commercially pure titanium against steel [51]. One study reports values five to seven times higher than the highest of these (85–107 $\times 10^{-4}$ mm^3/(N·m), derived from mass loss at 2 N) [49]; because the conversion could not be verified from the data given in the source, only the ranking of its manufacturing methods is used here, and it is not shown in Fig. 4. This spread reflects the tribosystem, i.e., counterface, contact geometry, load and wear-measurement method, at least as much as the material: for the same AM Ti-6Al-4V, changing only the counterface ball from SiC to WC increased the specific wear rate from 1.6 to 9.6 $\times 10^{-4}$ mm^3/(N·m) [53]. Absolute values from different studies are therefore not compared directly, and the observations below are based on comparisons within individual studies.

Within-study comparisons show that room-temperature hardness does not consistently rank wear resistance (Fig. 4; two studies that report no Vickers hardness values [53,58] are discussed in the text only). Lower wear of the harder material, as expected from Archard's relation [24], was reported for L-PBF commercially pure titanium compared with LENS, WAAM and cast material [51,55], and for heat-treated EB-PBF Ti-6Al-4V, in which the harder water-quenched conditions wore 9–18% less and the softer furnace-cooled conditions 15–27% more than the as-built state [58]. The opposite trend was found in other studies: as-built L-PBF and L-DED Ti-6Al-4V wore more than the softer wrought alloy in pin-on-ring tests [49], L-PBF Ti-6Al-4V (340 HV) wore more than cast material (290 HV) against WC [43] and against four different carbide counterfaces [53], and the softest heat-treated condition of EB-PBF Ti-6242 showed the lowest wear rate [59]. For L-PBF, EB-PBF and wrought Ti-6Al-4V tested under identical conditions, the ranking changed with the normal load (2, 6 and 10 N in Fig. 4) and the wear rates differed by less than 25% despite hardness differences of about 100 HV [35,50]. These contradictory trends indicate that, at room temperature, the wear of titanium alloys is controlled by the formation and removal of transfer layers and third bodies rather than by bulk hardness alone [29,50]. Features of the as-built microstructures, such as α′ martensite, residual stresses and porosity, act in both directions: they raise the hardness but can also promote subsurface cracking and the generation of third bodies [53,72,73]. Where AM and conventionally processed materials were tested under identical conditions, the specific wear rate of the AM material ranged from about 0.6–2.1 times that of the conventional material [35,49,50,53,55].

Beyond Ti-6Al-4V, the benchmark includes commercially pure titanium [51,55], near-α Ti-6242 [59], a metastable β Ti–Nb–Zr–Ta alloy [54] and γ-TiAl [32,56] (Table 2). The γ-TiAl alloys showed specific wear rates of 0.6–2.6 $\times 10^{-4}$ mm^3/(N·m) at hardnesses of only 257–295 HV [32,56]. For the metastable β alloy, the addition of Si changed the specific wear rate by only about 1%, at a sliding speed of 5 mm/min that is two to four orders of magnitude lower than in the other tests [54]; these values are listed for completeness but not compared quantitatively. Alloys were compared within the same study in only two cases: γ-TiAl wore 33–64% less than conventionally processed Ti-6Al-4V but showed higher coefficients of friction [56], whereas Ti-6Al-4V wore less and showed lower friction than the β Ti–Nb–Zr–Ta alloys [54]. Post-build heat treatments changed the room-temperature wear rate by up to a factor of about 2.4 [52,58,59], and among the thermal treatments of L-PBF Ti-6Al-4V, cryogenic treatment gave the lowest wear [57].

4.2. Effect of temperature on wear

Table 3 compiles the elevated-temperature data of the included studies, and Fig. 5 shows the specific wear rates of the tests performed in air, grouped by manufacturing method (AM technique or conventional processing), with the counterface material indicated by colour. As at room temperature, absolute values from different studies are not compared directly; the temperature effect is assessed within each study.

Table 1
Comparison of AM processes for Ti-6Al-4V (WAAM: Ti-6Al-4V and TA15) [13,16–18,22,35,49,50].

	L-PBF (SLM, DMLS)	EB-PBF (EBM)	DED (LMD, LENS)	WAAM (wire-arc DED)
Cooling Rate	Very High (10^3–10^8 K/s)	Moderate	High (10^2–10^4 K/s)	Low
Dominant Phase	Acicular Martensite (α′)	Near-equilibrium lamellar α + β (Widmanstätten)	Mixed α′ + α + β	Lamellar / basketweave α + β
Grain Morphology	Fine columnar prior-β grains	Coarser columnar grains	Large columnar grains	Coarse columnar prior-β grains
Typical Hardness	High (~370–430 HV)	Medium (~330–370 HV)	Medium (~350–410 HV)	Medium (~340–420 HV)
Wear Implication	Highest hardness, but wear rate not systematically lower than EB-PBF or wrought [35,50]	Higher ductility, lower hardness; wear rates similar to L-PBF [35,50]	Lack-of-fusion defects can supply third bodies [16]	Few tribological data [17,18]

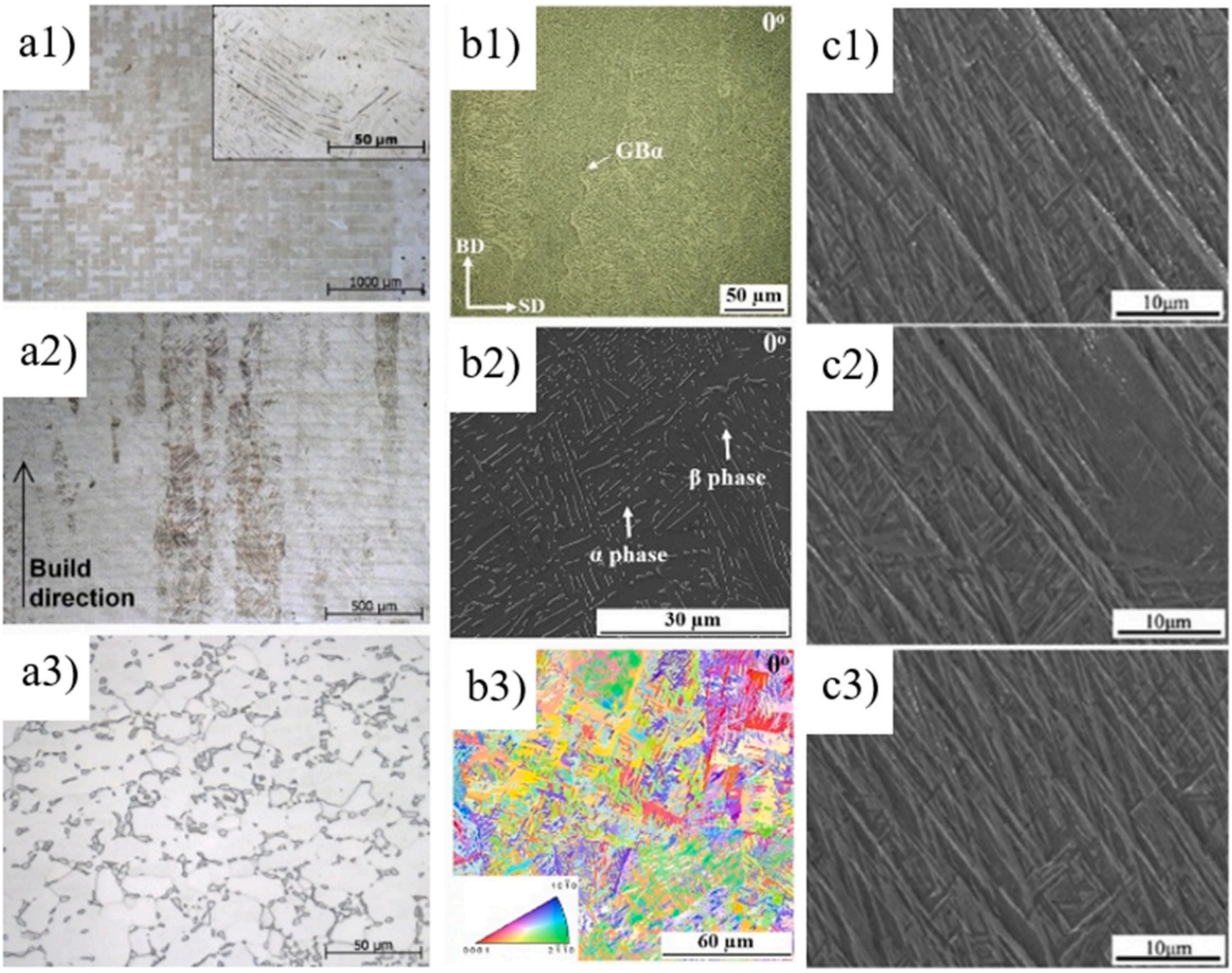


Fig. 3. Comparative microstructural features of Ti-6Al-4V: (a1, a2) top and side views of as-built L-PBF material with a fully martensitic (α′) structure within columnar prior-β grains and (a3) the conventionally processed reference material (α light, β dark), (b1, b2, b3) EB-PBF displaying a coarser lamellar structure, and (c1, c2, c3) DED showing a characteristic basket-weave morphology. Panels (a1–a3), (b1–b3) and (c1–c3) reproduced from [20], [78] and [79], respectively, with permission from Elsevier.

Across the dataset, the specific wear rate did not follow a single temperature dependence: depending on the tribosystem, it increased, decreased or changed non-monotonically between room temperature and 600–750 °C (Fig. 5).

The largest increases were reported against a SiC ball, where the specific wear rate of L-PBF Ti-6Al-4V rose from 7.0 to 16.2 × 10^{-4} mm^3/(N·m) between 25 and 550 °C [28], and against an Fe-based superalloy ball, where it increased about fivefold between 25 and 750 °C, mainly above 450 °C [27]. In pin-on-disc tests against EN31 steel, annealed L-PBF Ti-6Al-4V wore 6.6–8.1 times faster at 450 °C than at 150 °C [44], whereas as-built L-PBF material showed only a moderate increase (0.55–0.99 × 10^{-4} mm^3/(N·m), 28–450 °C) [33]. Against WC–Co and WC balls, the specific wear rate remained within about ±40% of the room-temperature value up to 600 °C in two studies [35,43], whereas in a third it changed by about 20% or less up to 400 °C and was about three times higher at 600 °C [36]. Decreasing wear with temperature was found mainly against Al_2O_3: for EB-PBF Ti-6Al-4V, the specific wear rate decreased by about 80% between 23 and 400 °C before rising again at 500 °C [37], and for EB-PBF Ti-6242 it decreased by about 10% [31] and, for a ground surface, by about 40% up to 450 °C, whereas a ground and tumble-finished surface showed no consistent trend [38]. The same EB-PBF Ti-6Al-4V sliding against a steel ball showed a similar pattern, with the lowest wear rates at 200–400 °C [37]. The reasons for these differences, namely the formation and stability of tribo-layers and the softening of the near-surface material, are discussed in Section 4.5.

Where AM and conventionally processed materials were tested under identical conditions, the temperature dependence of the manufacturing methods was similar. L-PBF, EB-PBF and wrought Ti-6Al-4V differed by at most about 30% at each temperature up to 600 °C [35]; L-DED Ti-6Al-4V wore 9–15% less than wrought material at all temperatures [36]; and stress-relieved L-PBF Ti-6Al-4V wore 44–61% more than cast material at all temperatures [43]. Within these studies, the effect of the manufacturing method was therefore smaller than the effects of temperature and counterface; the ranking of the manufacturing methods was preserved at all temperatures in [36] and [43], whereas the small differences in [35] changed order with temperature.

Several studies are listed in Table 3 but not shown in Fig. 5. Three report wear only as wear depth or mass loss [32,34,46]; in one of them, the maximum wear depth at 600 °C was about 53% lower than the peak value at 100 °C (113 versus 242 µm), which the authors attributed to a WO_3-containing film detected by XPS at ≥ 500 °C [34]. Two further studies are used only for within-study trends, because their reported specific wear rates are inconsistent with the wear depths given in the same study [39] or about four orders of magnitude lower than all other

Table 2
Room-temperature dry sliding data of the benchmark set. Where several materials are listed, values are given in the same order, separated by "/".

Manufacturing method / alloy / condition	Counterface, configuration	F (N); v (m/s); S (m)	Hardness (HV)	SWR ($\times 10^{-4}$ mm^3/(N·m))	CoF	Reported wear mechanisms[g]	Ref.
WAAM Ti-6Al-4V, three heat inputs	EN31 disc, pin-on-disc	9.8–49; 1–2; 3000	407–422	2.0–5.0[a]	0.30–0.43	Adhesive, abrasive (low heat input); oxidative (high heat input)	[17]
L-PBF / L-DED / wrought Ti-6Al-4V	1045 steel ring, pin-on-ring	2; 0.24; 434	~360 / ~400 / ~300	104 / 107 / 85[a,c]	n.r.	Adhesive, abrasive (L-DED, wrought: + oxidative)	[49]
L-PBF / EB-PBF / wrought Ti-6Al-4V	WC–Co ball, reciprocating	2–10; 0.04–0.16; 500	428 / 359 / 324	3.5–9.5 / 4.0–9.0 / 4.0–7.6	g.o.[e]	Adhesive, abrasive	[50]
L-PBF/ LENS / WAAM CP-Ti	Hardened steel disc, pin-on-disc	30; 0.54; 250	229 / ~201 / 190	9.5 / 13 / 16[a]	n.r.	Abrasive, delamination	[51]
EB-PBF Ti-48Al-2Cr-2Nb	ZrO_2 ball, ball-on-disc	15–80; n.r.; n.r.	282–295	2.0–2.6	0.44–0.54	Abrasive; + adhesive at high load	[32]
EB-PBF Ti-6Al-4V, furnace heat treatments	Si_3N_4 ball, reciprocating	5; 0.01; 18	332–349	1.9–4.5	0.45–0.52	Adhesive, abrasive (HT9: adhesive, oxidative)	[52]
AM / cast Ti-6Al-4V	B_4C, SiC, WC, TiC balls, reciprocating	5; 0.02; 36	5.61 / 5.51 GPa[d]	1.6–9.6 / 0.8–6.2	0.31–0.49 / 0.21–0.37	Abrasive, three-body abrasion; lubricating tribo-layer (vs SiC)	[53]
L-PBF TNZT / TNZTS (Ti-6Al-4V)	Si_3N_4 ball, reciprocating	15; 8×10^{-5}; n.r.	n.r.	0.009 / 0.009 (0.003)	0.72 / 0.70 (0.47)	Oxidative (TNZT; reduced in TNZTS)	[54]
L-PBF / cast CP-Ti	Hard-faced steel disc, pin-on-disc	15–30; 0.57; ~509	261 / 210	0.38–0.49 / 0.61–0.66[a]	n.r.	Abrasive, oxidative	[55]
EB-PBF γ-TiAl	HCHCr steel disc, pin-on-disc	20–40; 1–2; 2000	257	0.62–1.02	0.29–0.45	Abrasive	[56]
L-PBF Ti-6Al-4V, SR / HT / cryogenic	EN31 disc, pin-on-disc	n.r.; 1.5; 2000	n.r.	r.o.[b]	g.o.[e]	Abrasive, delamination, ploughing	[57]
EB-PBF Ti-6Al-4V, HT + WQ / FC	EN31 disc, pin-on-disc	10–49; 1.5; 2639	n.r.	r.o.[b]	g.o.[e]	Abrasive (1040 °C FC: adhesive, delamination)	[58]
EB-PBF Ti-6242, as-built / 960 °C / 1050 °C	ZrO_2 ball, pin-on-disc	20; 0.11; 1000	416 / 341 / 372	3.5 / 1.9 / 2.7[f]	0.54 / 0.40 / 0.47	Abrasive (as-built); adhesive (960 °C); adhesive, abrasive, micro-cutting (1050 °C)	[59]

n.r. = not reported. [a] Calculated from mass loss using the alloy density. [b] r.o. = relative only; the source reports percentage changes with respect to the as-built condition. [c] Not shown in Fig. 4 (see text). [d] Nanoindentation hardness. [e] g.o. = graphical only; no numerical value reported. [f] Converted from mm^3/(N·min). [g] As stated in the conclusions of each source, or in the worn-surface analysis where the conclusions name no mechanism.

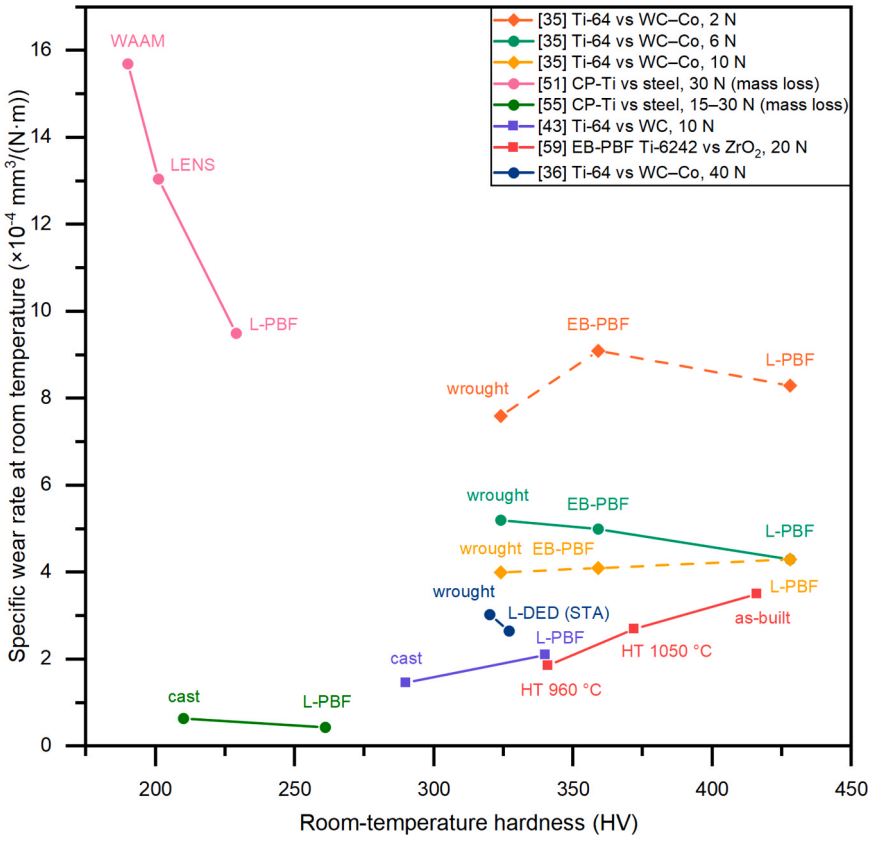


Fig. 4. Specific wear rate versus hardness at room temperature (dry sliding). Each line connects materials tested under identical conditions in the same study, and the labels give the material variant; for [35], the three lines correspond to normal loads of 2, 6 and 10 N. Circles: the harder material wore less; squares: the harder material wore more; dashed lines: no consistent order. Data of [49] are not shown (see text). All data refer to room-temperature tests. Ti-64 = Ti-6Al-4V.

Table 3
Elevated-temperature dry sliding data of the included studies. Values in the SWR and CoF columns are given in the order of the test temperatures, separated by "/".

Manufacturing method / alloy / condition	Counterface, configuration	F (N); v (m/s); S (m)	T (°C)	SWR ($\times 10^{-4}$ mm^3/(N·m))	CoF	Reported wear mechanisms[j]	Ref.
EB-PBF Ti-6242, as-built[b]	Al_2O_3 ball, ball-on-disc	5; 0.1; 180	25 / 250 / 450	4.2 / 4.0 / 3.8	0.50 / 0.58 / 0.51	Abrasive; + adhesive, oxidative (250 °C); + oxidative (450 °C)	[31]
EB-PBF Ti-48Al-2Cr-2Nb	18Ni300 ring, ring-on-disc	200; n.r.; n.r.	200 / 400 / 600 / 800	n.r.[d]	0.69 / 0.66 / 0.56 / 0.49	Abrasive, adhesive, oxidative (200–400 °C); adhesive (600 °C); abrasive, softening-induced peeling (800 °C)	[32]
L-DED TC11, as-deposited	GCr15 ball, ball-on-disc	100; n.r.; n.r.	25 / 500	n.r.[d]	n.r.	Abrasive, delamination, oxidative (mild at 25 °C, severe at 500 °C)	[46]
L-PBF Ti-6Al-4V, as-built	EN31 disc, pin-on-disc	30; 2.0; 2000	28 / 150 / 300 / 450	0.55 / 0.77 / 0.84 / 0.99	0.20 / 0.28 / 0.37 / 0.39	Abrasive (28 °C); oxidative, delamination, three-body abrasion (≥ 150 °C)	[33]
L-PBF Ti-6Al-4V, 800 °C/8 h	WC–Co ball, reciprocating	50; 0.12; 216	25 / 100 / 200 / 300 / 400 / 500 / 600	n.r.[d]	0.98 / 0.90 / 0.91 / 0.88 / 0.97 / 0.90 / 0.86	Adhesive, three-body abrasion; WO_3-containing film (XPS, ≥ 500 °C); Co diffusion (600 °C)	[34]
L-PBF Ti-6Al-4V, as-built	Fe-based superalloy (GH2132) ball, reciprocating	50; 0.02; 12[f]	25 / 350 / 450 / 550 / 650 / 750	4.2 / 4.9 / 7.0 / 14.7 / 18.7 / 20.6	0.39 / 0.43 / 0.44 / 0.48 / 0.49 / 0.50	Abrasive, adhesive (≤ 350 °C); delamination, abrasive (450 °C); oxidative, oxide-layer spalling (≥ 550 °C)	[27]
L-PBF Ti-6Al-4V, as-built	WC–Co ball, reciprocating	10; 0.1; 500[f]	25 / 200 / 400 / 600	4.3 / 5.4 / 4.5 / 3.6	0.67 / 0.76 / 0.72 / 0.69	Not named; oxide–debris layer on the track (≥ 200 °C)	[35]
EB-PBF Ti-6Al-4V, as-built	WC–Co ball, reciprocating	10; 0.1; 500[f]	25 / 200 / 400 / 600	4.1 / 5.6 / 4.3 / 4.7	0.62 / 0.76 / 0.75 / 0.85	Not named; oxide–debris layer on the track (≥ 200 °C)	[35]
Wrought Ti-6Al-4V, annealed	WC–Co ball, reciprocating	10; 0.1; 500[f]	25 / 200 / 400 / 600	4.0 / 5.3 / 3.8 / 4.6	0.63 / 0.78 / 0.75 / 0.84	Not named; oxide–debris layer on the track (≥ 200 °C)	[35]
L-DED Ti-6Al-4V, STA	WC–Co ball, ball-on-disc	40; 0.19; 339	25 / 200 / 400 / 600	2.6 / 3.1 / 3.1 / 8.7	0.40 / 0.41 / 0.32 / 0.24	Abrasive (25 °C); oxide-film peeling (200 °C); oxidative, fatigue (≥ 400 °C)	[36]
Wrought Ti-6Al-4V	WC–Co ball, ball-on-disc	40; 0.19; 339	25 / 200 / 400 / 600	3.0 / 3.6 / 3.4 / 9.6	0.39 / 0.41 / 0.41 / 0.38	Abrasive (≤ 200 °C); oxidative, fatigue (≥ 400 °C)	[36]
EB-PBF Ti-6Al-4V, as-built	Al_2O_3 ball, ball-on-disc	10; 0.1; 360	23 / 200 / 400 / 500	8.0 / 2.5 / 1.4 / 4.6	0.48 / 0.45 / 0.40 / 0.33	Abrasive (23 °C); abrasive, adhesive (200 °C); oxidative (≥ 400 °C)	[37]
EB-PBF Ti-6Al-4V, as-built	AISI 52100 steel ball, ball-on-disc	10; 0.1; 360	23 / 200 / 400 / 500	6.8 / 0.80 / 0.95 / 2.6	0.50 / 0.50 / 0.30 / 0.45	Adhesive, abrasive; + oxidative (500 °C)	[37]
EB-PBF Ti-6242, ground	Al_2O_3 ball, ball-on-disc	5; 0.1; 180	25 / 250 / 450	4.1 / 2.5 / 2.4	0.52 / 0.51 / 0.44	Ploughing, abrasive, adhesive (25 °C); ploughing, abrasive, oxidative (≥ 250 °C)	[38]
EB-PBF Ti-6242, ground + tumble finished	Al_2O_3 ball, ball-on-disc	5; 0.1; 180	25 / 250 / 450	2.1 / 3.2 / 2.4	0.39 / 0.53 / 0.40	Minor damage (25 °C); ploughing, abrasive, oxidative (≥ 250 °C)	[38]
L-PBF Ti-6Al-4V, as-built	Si_3N_4 ball, reciprocating	5–60; 0.1; 120	25 / 100 / 200 / 300 / 400	18–33 / 28–50 / 23–62 / 7–37 / 7–34[c]	0.41–0.44 / 0.45–0.52 / 0.44–0.54 / 0.43–0.49 / 0.42–0.46	Abrasive (25 °C); three-body abrasion (100 °C); adhesive (200 °C); oxidative at ≥ 20 N, adhesive at 5 N (300–400 °C)	[39]
L-PBF Ti-6Al-4V, as-built[g]	Al_2O_3 ball, ball-on-disc, high vacuum	10; n.r.; n.r.	28 / 400 / 850	0.07 / 0.85 / 2.7	0.52 / 0.18 / 0.09	Abrasive (28 °C); adhesive (≥ 400 °C)	[40]
L-PBF Ti-6Al-4V, HT-1 (sub-transus)[g]	Al_2O_3 ball, ball-on-disc, high vacuum	10; n.r.; n.r.	28 / 400 / 850	0.20 / 1.3 / 4.2	0.48 / 0.10 / 0.07	Abrasive (28 °C); adhesive (≥ 400 °C)	[40]
L-PBF Ti-6Al-4V, HT-2 (super-transus)[g]	Al_2O_3 ball, ball-on-disc, high vacuum	10; n.r.; n.r.	28 / 400 / 850	0.13 / 0.87 / 3.3	0.45 / 0.08 / 0.05	Abrasive (28 °C); adhesive (≥ 400 °C)	[40]
L-PBF Ti-6Al-4V, 800 °C/2 h	Hardened steel disc, pin-on-disc	9.8; 1.0[k]; n.r.	350 / 450 / 550 / 600	1.6 / 0.54 / 0.39 / 0.44[a]	0.62 / 0.34 / 0.28 / 0.38	Adhesive, abrasive (350 °C); oxidative (450–550 °C); oxidative, oxide spallation, three-body abrasion (600 °C)	[41]
L-PBF Ti-6Al-4V, as-built	EN31 disc, pin-on-disc	50; n.r.; 1500	28 / 100 / 200 / 300 / 400 / 500 / 600	~10^{-4} of other data[c,e]	0.39 / 0.37 / 0.37 / 0.36 / 0.34 / 0.33 / 0.43	Adhesive, oxidative (≤ 200 °C); oxidative, three-body abrasion (300–400 °C); oxidative, delamination (500–600 °C)	[42]
L-PBF Ti-6Al-4V, 790 °C/2 h	WC ball, ball-on-disc	10; n.r.; 500	25 / 300 / 600	2.1 / 2.4 / 2.9	0.26 / 0.35 / 0.29	Abrasive, oxidative, adhesive	[43]
Cast Ti-6Al-4V	WC ball, ball-on-disc	10; n.r.; 500	25 / 300 / 600	1.5 / 1.5 / 1.9	0.25 / 0.34 / 0.27	Abrasive, oxidative, adhesive	[43]
L-PBF Ti-6Al-4V, 860 °C/2 h	EN31 disc, pin-on-disc	50; 1.5; 750[f]	150 / 250 / 350 / 450	1.2 / 2.1 / 4.3 / 8.1[a]	0.37 / 0.34 / 0.28 / 0.22	Abrasive (150 °C); oxidative, delamination (250–350 °C); adhesive, plastic deformation (450 °C)	[44]
L-PBF Ti-6Al-4V, 960 °C/2 h	EN31 disc, pin-on-disc	50; 1.5; 750[f]	150 / 250 / 350 / 450	1.3 / 2.9 / 5.0 / 10.9[a]	0.36 / 0.32 / 0.27 / 0.22	Abrasive (150 °C); oxidative, delamination (250 °C); abrasive, plastic deformation, delamination (350 °C); adhesive, plastic deformation (450 °C)	[44]
L-DED Ti-6Al-4V, as-deposited	GCr15 disc, pin-on-disc	50; n.r.; n.r.	400	1.6	0.66	Adhesive, abrasive, oxidative	[61]
WAAM TA15, as-deposited[h]	Si_3N_4 ball, small-amplitude reciprocating	10; 0.006; 10.8	25 / 200 / 400 / 600 / 800 / 1000	0.08 / 0.08 / 0.21 / 0.08 / 0.06 / 2.5	0.60 / 0.58 / 0.55 / 0.50 / 0.56 / 0.67	Abrasive (≤ 200 °C); oxidative, abrasive (400–800 °C); delamination, oxidative (1000 °C)	[18]
L-PBF Ti-6Al-4V, as-built	SiC ball, reciprocating	50; 0.02; 72[f]	25 / 350 / 550	7.0 / 9.1 / 16.2	0.42 / 0.43 / 0.47	Three-body abrasion (25 °C); oxidative, adhesive (≥ 350 °C)	[28]
L-DED Ti-6Al-4V, as-deposited	Si_3N_4 ball, reciprocating	20; 0.01; 18[i]	25 / 300	3.6 / 1.7	0.42 / 0.57	Adhesive (25 °C); abrasive, adhesive (300 °C)	[45]

n.r. = not reported. [a] Calculated from mass loss using the alloy density. [b] Mean of horizontal and vertical builds (difference < 3%). [c] Not shown in Fig. 5 (see text). [d] Wear reported only as wear depth [32,34] or mass loss without track radius [46]. [e] Values printed in the source are about four orders of magnitude lower than in all other studies. [f] Further loads [27,35,44] or sliding durations [28] are listed in Table S1a. [g] Tested in high vacuum (10^{-5}–10^{-6} mbar); not shown in Fig. 5. [h] Small-amplitude (fretting-like) reciprocating test; not shown in Fig. 5. [i] Room-temperature and 300 °C tests run on different tribometers; v and S refer to the room-temperature test. [j] As reported by the authors for each test temperature. [k] Methods state 1.0 m/s; results state 4 m/s.

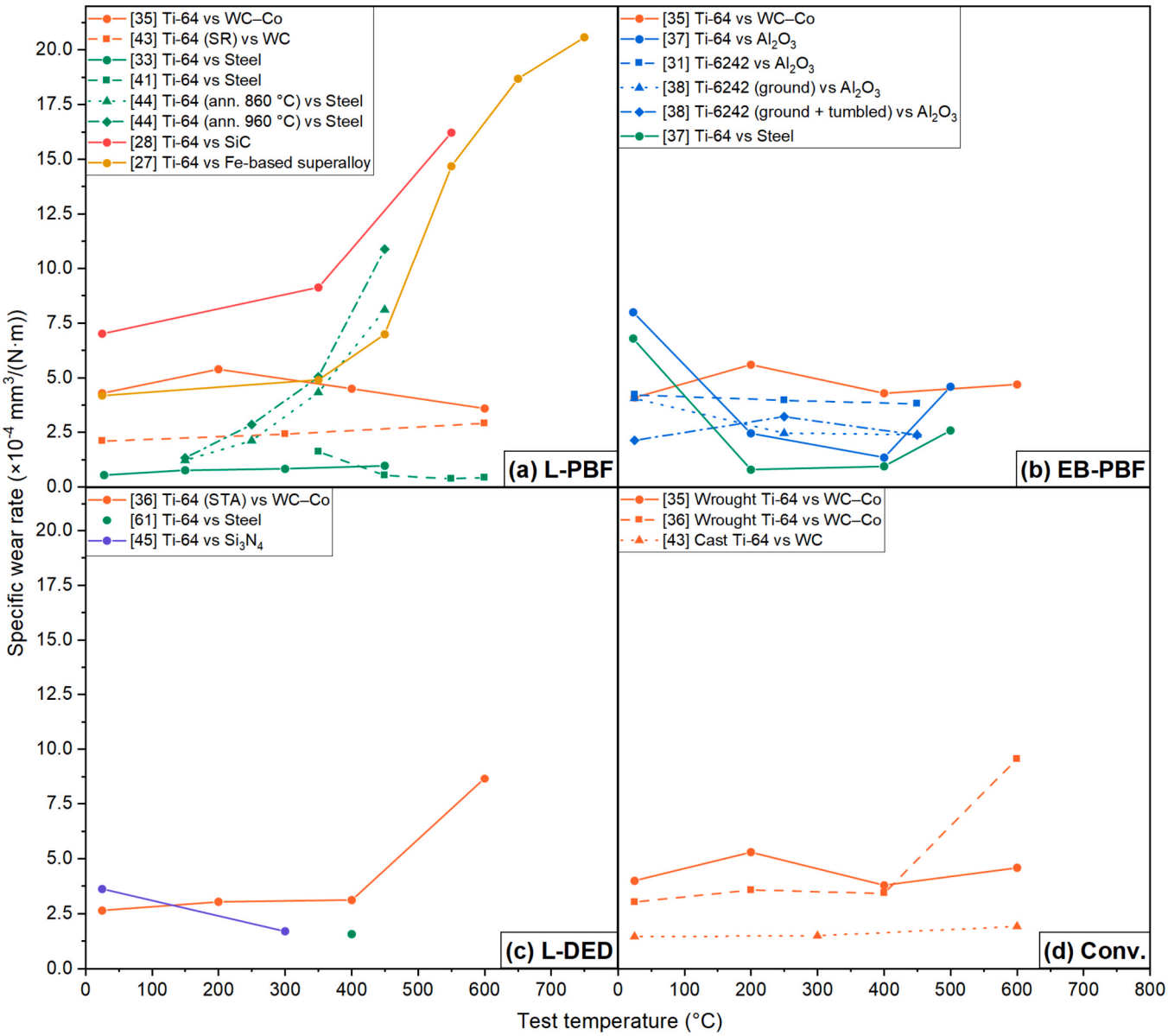


Fig. 5. Specific wear rate versus test temperature for dry sliding in air, grouped by manufacturing method: (a) L-PBF, (b) EB-PBF, (c) L-DED and (d) wrought or cast reference material. Line colour denotes the counterface material; each line connects the data of one material condition in one study. One test condition is shown per study [35]: 10 N; [27], [44]: 50 N; [28]: 60 min; [31]: mean of horizontal and vertical builds); further conditions are listed in Table S1a. Studies without specific wear rates [32,34,46], data of [39] and [42] (see text), tests in high vacuum [40] and small-amplitude tests [18] are not shown. Ti-64 = Ti-6Al-4V.

data [42] (Section 2.2). Tests in high vacuum, in which the specific wear rate increased 21–38-fold between 28 and 850 °C while the coefficient of friction decreased to 0.05–0.09 [40], and small-amplitude reciprocating tests of WAAM TA15, in which the wear rate remained low up to 800 °C and increased about thirtyfold at 1000 °C [18], represent different tribosystems and are discussed in Section 4.5.

4.3. Effect of temperature on friction

Fig. 6 shows the coefficients of friction reported for the elevated-temperature tests in air, in the same layout as Fig. 5. Most values lie between 0.2 and 0.6. Higher values were reported for reciprocating tests against WC–Co balls (0.62–0.98) [34,35] and for ring-on-disc tests of γ-TiAl against maraging steel (0.49–0.69) [32], indicating that the counterface and the contact configuration affect the friction level more than the test temperature. As for the wear rate, no common temperature dependence was found. The coefficient of friction decreased with temperature in several studies, for example from 0.37 to 0.22 between 150 and 450 °C against EN31 steel [44] and from 0.48 to 0.33 between 23 and 500 °C against Al_2O_3 [37], whereas it increased in others, for example from 0.20 to 0.39 between 28 and 450 °C against EN31 steel [33] and from 0.39 to 0.50 between 25 and 750 °C against an Fe-based

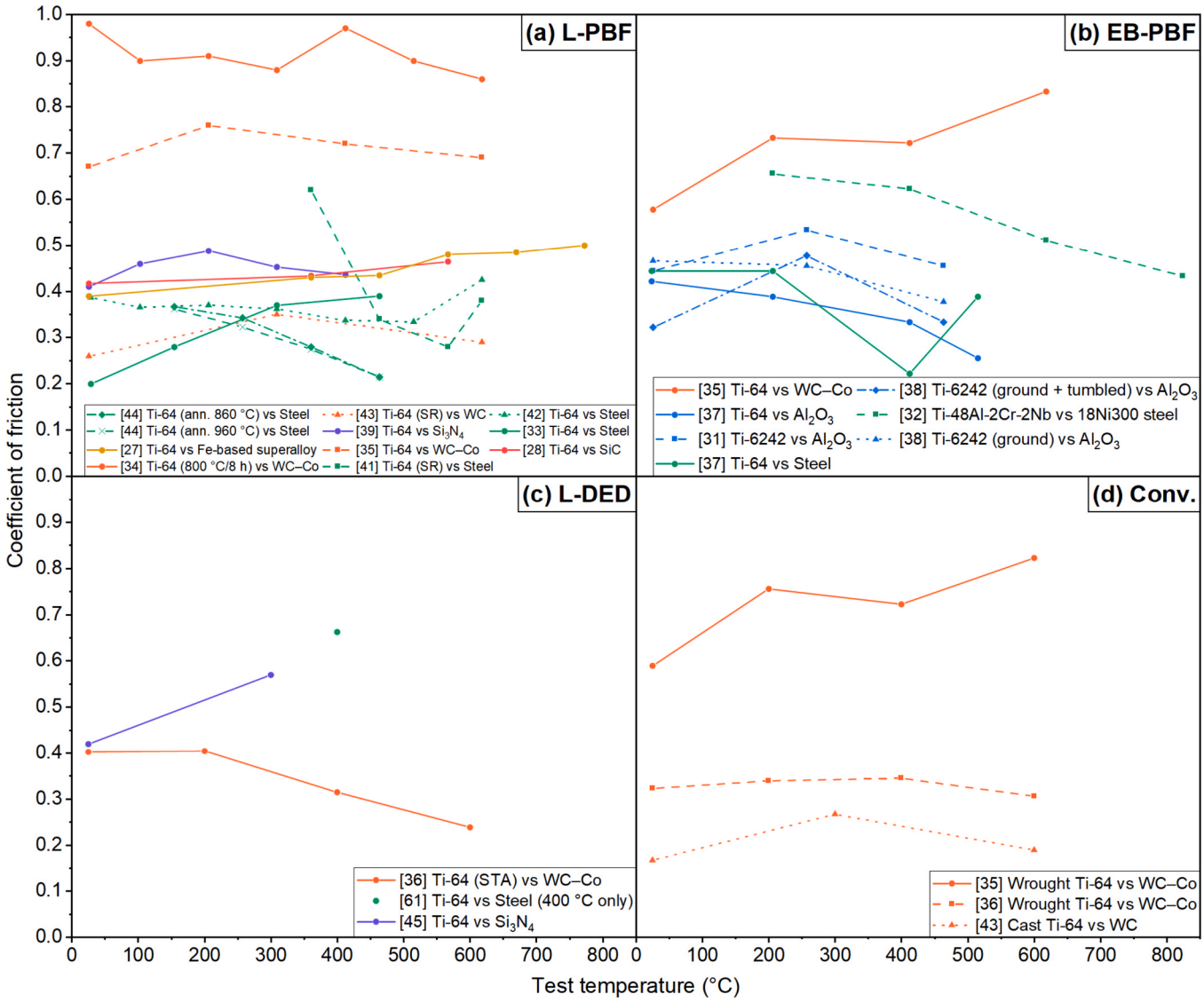


Fig. 6. Coefficient of friction versus test temperature for dry sliding in air, grouped by manufacturing method: (a) L-PBF, (b) EB-PBF, (c) L-DED and (d) wrought or cast reference material. Line colour denotes the counterface material; each line connects the data of one material condition in one study. One test condition is shown per study [35]: 10 N; [39]: 20 N; [27], [44]: 50 N; [28]: 60 min; [31]: horizontal build); further conditions are listed in Table S1a. Tests in high vacuum [40] and small-amplitude tests [18] are not shown. Ti-64 = Ti-6Al-4V.

superalloy [27]. In most studies, the coefficient of friction changed by less than about 0.2 over the tested temperature range, whereas the specific wear rate of the same tests changed by up to several times (Table 3). In the WC–Co tests in which a WO_3-containing film was detected at $\geq$ 500 °C, the coefficient of friction remained between 0.86 and 0.90 [34].

Changes in friction and wear with temperature were often not correlated. In the tests of [44], the coefficient of friction decreased by about 40% between 150 and 450 °C while the specific wear rate increased 6.6–8.1-fold; L-DED Ti-6Al-4V showed its lowest coefficient of friction (0.24) at 600 °C, where its wear rate was about three times the room-temperature value [36]; and against an Fe-based superalloy, the coefficient of friction increased by about 30% while the wear rate increased about fivefold [27]. The clearest example is provided by tests in high vacuum, in which the coefficient of friction decreased to 0.05–0.09 at 850 °C while the specific wear rate increased 21–38-fold [40]. A low coefficient of friction at elevated temperature therefore does not by itself indicate low wear, and the two quantities are discussed separately in this review. Where manufacturing methods were compared under identical conditions, the coefficients of friction differed by 0.05 or less in most cases; larger differences appeared only at 400–600 °C, where L-DED Ti-6Al-4V showed lower friction than wrought material (0.24–0.32 versus 0.38–0.41) although both wore at similar rates [36], and at 600 °C for L-PBF compared with EB-PBF and wrought Ti-6Al-4V [35]. All of these comparisons of manufacturing methods were performed against WC–Co or WC counterfaces [35,36,43]; for other counterfaces, no data are available to compare manufacturing methods under identical conditions.

4.4. *Effects of normal load and sliding time*

Four studies varied the normal load at several test temperatures [27,35,39,44]. Because the specific wear rate is normalized by the load, a wear volume proportional to the load, as assumed in Archard's relation [24], gives a ratio of 1 between the specific wear rates at the higher and the lower load. Fig. 7a shows that this ratio deviated from 1 in two opposite directions. In pin-on-disc tests of annealed L-PBF Ti-6Al-4V against EN31 steel, increasing the load from 50 to 75 N raised the specific wear rate by a factor of 1.03–1.95, depending on temperature and annealing condition [44]. In the three ball-on-flat reciprocating studies,

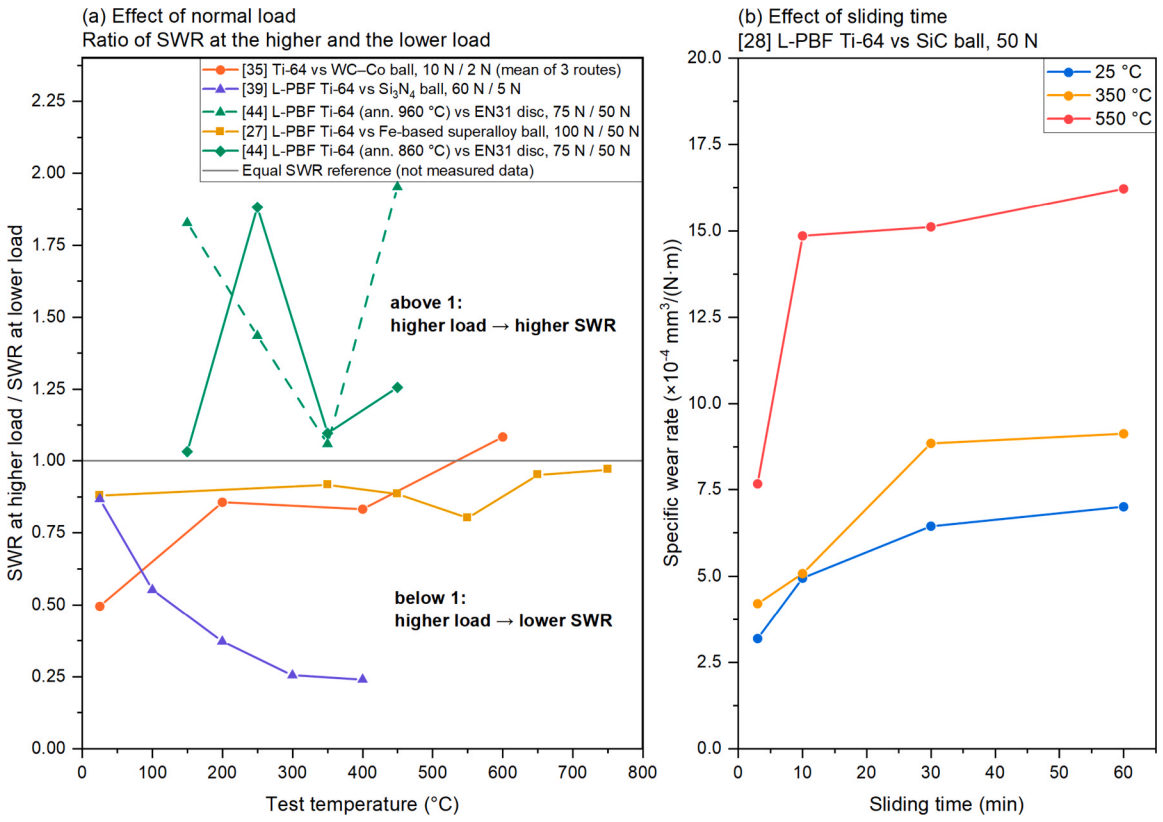


Fig. 7. Effects of normal load and sliding time at constant test temperature. (a) Ratio of the specific wear rates measured at the higher and the lower normal load in the same study, plotted against test temperature; a ratio of 1 corresponds to a wear volume proportional to the load. For [35], the ratio refers to the mean of L-PBF, EB-PBF and wrought Ti-6Al-4V; for [39], it refers to the lowest and highest loads (5 and 60 N). (b) Specific wear rate of L-PBF Ti-6Al-4V against a SiC ball at 50 N as a function of sliding time [28]. Ti-64 = Ti-6Al-4V.

the specific wear rate at the higher load was lower than at the lower load in all conditions but one, i.e., the wear volume mostly increased less than proportionally with load [27,35,39]. The size of this effect depended on temperature in two of these studies: the ratio rose from 0.50 at room temperature to 1.08 at 600 °C for Ti-6Al-4V against WC–Co (10 versus 2 N) [35], and it fell from 0.87 at room temperature to 0.24–0.26 at 300–400 °C against Si_3N_4 (60 versus 5 N) [39]. In the latter study, the specific wear rate at 300–400 °C was highest at 20 N, and the authors reported oxidative wear at loads of 20 N and above but adhesive wear at 5 N [39]. Against an Fe-based superalloy, the ratio remained between 0.80 and 0.97 from 25 to 750 °C [27]. The two groups differ in contact configuration (conformal pin-on-disc contact at 50–75 N versus non-conformal ball contact), but the number of studies is too small to attribute the difference to this factor. Since the load effect changed with temperature in three of the four studies, load effects determined at a single temperature cannot be transferred to other temperatures.

Only one study varied the sliding time at several temperatures (Fig. 7b) [28]. For L-PBF Ti-6Al-4V against a SiC ball, the specific wear rate increased with sliding time at all temperatures, from 3.2 to 7.0×10^{-4} $mm^3/(N{\cdot}m)$ at 25 °C and from 7.7 to 16.2×10^{-4} $mm^3/(N{\cdot}m)$ at 550 °C between 3 and 60 min. At 550 °C, most of this increase occurred within the first 10 min. The ratio between the values at 550 °C and 25 °C remained between 2.3 and 3.0 for all sliding times, so the temperature ranking did not depend on test duration, whereas the absolute values did. At 350 and 550 °C, the authors reported a transition from adhesive wear with slight oxidation during running-in to severe oxidative and adhesive wear as the sliding time increased, and attributed the slower growth of the wear rate to a continuous tribo-layer [28]. Since the sliding distances of the included studies range from about 4–2000 m (Table 3 and Table S1a), differences in test duration contribute to the scatter of absolute wear rates between studies.

4.5. Tribo-layers and the role of hardness

Table 4 summarizes the evidence for tribo-layers in the elevated-temperature studies. Of the 19 studies performed in air, five identified oxide phases on the worn surface or in the debris by XRD or Raman spectroscopy [18,33,37,38,42], two determined chemical states by XPS [28,34], ten relied on EDS only (in one study on the counterface only [44]), and two on SEM observation without chemical analysis [41,45]. In all studies with phase identification, the tribo-layers contained TiO_2; anatase was identified in three studies [18,37,38] and rutile in two [18, 37], with rutile dominating at 600 °C and above in the one study extending to 1000 °C [18]. Against steel counterfaces, transferred iron oxides (α-Fe_2O_3, Fe_3O_4) were identified in two studies [37,42], whereas another found no Fe_2O_3 on the worn surface [33]; Al_2O_3 and SiO_2 were also reported in one of these studies [42]. WO_3 was detected by XPS in one study with a WC–Co counterface at ≥ 500 °C [34]; this indicates the oxidation state of tungsten but not the crystal structure of the oxide. The thickness of the tribo-layers was rarely quantified (about 10 μm at 650–750 °C in [27]).

Most authors attributed a protective role to the tribo-layers (Table 4), but their presence did not consistently coincide with lower wear than at room temperature. Decreases in the specific wear rate accompanied TiO_2-containing layers against Al_2O_3 and steel balls (by 70–90% at 200–400 °C [37]; about 40% at 450 °C for a ground surface [38]) and in the small-amplitude tests at 600–800 °C [18]. In other studies, layers of similar composition were present while the specific wear rate increased, by about 80% between 28 and 450 °C [33] and 2.3-fold between 25 and 550 °C [28]; in the latter, the authors attributed the protective effect to a slower growth of wear with sliding time rather than to lower wear than at room temperature (Section 4.4). Layers that formed above 450 °C against an Fe-based superalloy failed by cracking and spalling, while the

Table 4
Evidence for tribo-layers in the elevated-temperature studies, graded according to Section 2.4: phase (XRD or Raman spectroscopy of the worn surface or debris), chemical state (XPS), elemental (EDS only) and morphological (SEM observation only).

Manufacturing method / alloy	Counterface	T with reported layer (°C)	Technique (worn surface)	Identified phases / chemical states	Evidence level	Role attributed by the authors	Ref.
EB-PBF Ti-6242	Al_2O_3 ball	250, 450	EDS	O enrichment (TiO_2 inferred)	Elemental	Unstable at 250 °C; protective at 450 °C	[31]
EB-PBF Ti-48Al-2Cr-2Nb	18Ni300 ring	200–800	EDS	O enrichment; elements of both bodies	Elemental	Compacted layer protective at 400 °C; peels at higher T	[32]
L-DED TC11	GCr15 ball	500	EDS	O enrichment	Elemental	Protective; fragments act as third bodies	[46]
L-PBF Ti-6Al-4V	EN31 disc	28–450	XRD, EDS	TiO_2; no Fe_2O_3	Phase	No significant effect on wear resistance	[33]
L-PBF Ti-6Al-4V	WC–Co ball	≥ 500	XPS, EDS	WO_3; CoO (600 °C)	Chemical state	Lubricating WO_3 film; reduces wear	[34]
L-PBF Ti-6Al-4V	Fe-based superalloy ball	≥ 450	EDS (SEM, TEM)	Mixed Al, Ti, V oxides; Al-rich surface	Elemental	Reduces adhesion; fails by cracking and spalling	[27]
L-PBF / EB-PBF / wrought Ti-6Al-4V	WC–Co ball	200–600	EDS	O enrichment	Elemental	Probably protective at 400–600 °C	[35]
L-DED / wrought Ti-6Al-4V	WC–Co ball	400–600	EDS	O enrichment	Elemental	Resists abrasion; cracking causes fatigue fracture	[36]
EB-PBF Ti-6Al-4V	Al_2O_3 ball; steel ball	200–500	Raman, EDS	TiO_2; rutile + anatase (steel ball, 500 °C); α-Fe_2O_3, Fe_3O_4 (steel ball, 400 °C)	Phase	Protective; fractured layer abrasive at 200 °C	[37]
EB-PBF Ti-6242	Al_2O_3 ball	250, 450	XRD, EDS	TiO_2 (anatase)	Phase	Unstable at 250 °C; protective, lubricating at 450 °C	[38]
L-PBF Ti-6Al-4V	Si_3N_4 ball	25–400	EDS, SEM cross-section	O enrichment	Elemental	Protective when dense (300–400 °C)	[39]
L-PBF Ti-6Al-4V	Al_2O_3 ball, high vacuum	–	EDS	No atmospheric oxidation	Control	No oxide role	[40]
L-PBF Ti-6Al-4V	Steel disc	350–600	SEM	Not identified	Morphological	Protective at 450–550 °C; spalls at 600 °C	[41]
L-PBF Ti-6Al-4V	EN31 disc	300–600	XRD, EDS	TiO_2, Ti_6O, Fe_3O_4, Al_2O_3, SiO_2	Phase	Lowers friction at 500 °C; oxide debris abrasive	[42]
L-PBF / cast Ti-6Al-4V	WC ball	25, 300, 600	EDS	O enrichment; W transfer	Elemental	Thin layers fracture (300 °C); thicker layers lower friction (600 °C)	[43]
L-PBF Ti-6Al-4V	EN31 disc	450 (on counterface)	EDS (counterface)	Transfer film on the disc; not identified	Elemental	Transfer film lowers friction	[44]
L-DED Ti-6Al-4V	GCr15 disc	400	EDS	O enrichment	Elemental	No role stated	[61]
WAAM TA15	Si_3N_4 ball	25–1000	XRD, Raman, EDS	TiO_2 (anatase + rutile; rutile strongest ≥ 600 °C); Ti_6O (25 °C); Al_2O_3 inferred from EDS (800 °C)	Phase	Non-protective ≤ 400 °C; protective at 800 °C; delaminates at 1000 °C	[18]
L-PBF Ti-6Al-4V	SiC ball	25, 350, 550	XPS, EDS	Ti^{4+} (TiO_2), Al^{3+} (Al_2O_3); Al^0 at 25 °C	Chemical state	Protective at 350–550 °C; fragmented at 25 °C	[28]
L-DED Ti-6Al-4V	Si_3N_4 ball	300	SEM	Not identified	Morphological	Protective barrier, solid lubricant (300 °C)	[45]

wear rate increased about fivefold [27], and the small-amplitude tests showed delamination of the layer and a thirtyfold increase in wear at 1000 °C [18]. Tests in high vacuum, in which atmospheric oxidation was absent, showed a 21–38-fold increase in the specific wear rate between 28 and 850 °C with adhesive wear [40]. This is consistent with a wear-limiting effect of oxide layers in air, although no tests in air were performed in the same study.

The contact pressure may explain part of this variation. In ball-on-flat tests, decreases of the specific wear rate with temperature were reported mainly at initial Hertzian pressures below about 1 GPa (Section 2.3) [31,35,37,38], and increases mainly above about 1.3 GPa [27,28,36,43]. Within one study, the decrease at 600 °C was largest at the lowest load: 47–58% at 2 N, compared with −20% to + 15% at 6 and 10 N [35]. Across all studies that reported specific wear rates at several temperatures, the ratio between the wear rates at the highest and the lowest test temperature tended to increase with the normal load (Spearman $\rho = 0.61$, $p = 0.03$, 13 studies), although the load is correlated with the counterface and the temperature range of the studies. This is consistent with a limited load-bearing capacity of tribo-layers, which depends on the support provided by the softening substrate. However, most low-pressure tests were performed against Al_2O_3, so the effects of pressure and counterface cannot be separated, and one study showed the largest decrease at the highest loads (40–60 N) [39]. Pin-on-disc tests with conformal contact are not included in this comparison, because their nominal pressures are not comparable with Hertzian pressures.

The strength of the substrate at the test temperature was, however, not measured in most studies: none of the included studies reported hot hardness values of the tested materials. The only elevated-temperature strength data were reported for L-PBF Ti-6Al-4V tested against SiC, for which the ultimate tensile strength decreased from about 1240 MPa at room temperature to 988 and 516 MPa at 350 and 550 °C, and the microhardness below the worn surface also decreased with temperature [28]. The corresponding increases in the specific wear rate (1.3-fold and 2.3-fold) were close to the reciprocal decreases in strength (1.26 and 2.40). If the hardness at the test temperature is assumed to scale with the tensile strength and the wear coefficient to remain constant, this agreement is consistent with Archard's relation [24]; since neither assumption was verified, and tribo-layers were present at all temperatures, the agreement is only qualitative and cannot be generalized from a single study. Room-temperature hardness, in contrast, did not rank the wear resistance at elevated temperature, as already observed at room temperature (Section 4.1): stress-relieved L-PBF Ti-6Al-4V (340 HV) wore 44–61% more than cast material (290 HV) at all temperatures [43]; in high vacuum, both heat-treated conditions, which were harder

than the as-built material, wore as much as or more than it at all temperatures [40]; and the ranking of L-PBF, EB-PBF and wrought Ti-6Al-4V changed with temperature [35]. Hot hardness or hot strength data of the tested materials are therefore needed to evaluate Archard-type relations at elevated temperature.

4.6. Temperature dependence of the reported wear mechanisms

Fig. 8 compiles the wear mechanisms reported for each test temperature, grouped by counterface material. A mechanism is shown as dominant only where the authors explicitly ranked it above the others (e.g., 'dominant', 'mainly' or 'primary') or named it as the only mechanism; where mechanisms were named without such a ranking, the point is shown as mixed, and the named mechanisms are indicated. Of the 91 study–temperature points, 32 had an explicitly stated dominant mechanism, 46 were mixed and 13 named no mechanism. Where a dominant mechanism was stated at room temperature, it was abrasive in seven of nine test series [28,31,33,36,37] and adhesive in two [34,45]. Oxidative wear was identified as dominant in four studies, from 150 °C [33], 400 °C [37], 450 °C [41] and 550 °C [27]; in two of these, the tribo-layer was documented by EDS or SEM only [27,41]. Adhesive wear was named in seven of the nine test series against steel counterfaces and identified as dominant at 400–450 °C in two studies [37,44], whereas against Al_2O_3 it was named only as a secondary mechanism, in the form of material transfer [31,37,38].

The counterface changed the reported mechanism even for the same material and test conditions: EB-PBF Ti-6Al-4V showed predominantly oxidative wear at 400–500 °C against Al_2O_3, but predominantly adhesive wear at 400 °C against a steel ball [37]. The sequences were also not monotonic: L-PBF Ti-6Al-4V annealed at 860 °C showed predominantly adhesive wear at 450 °C after oxidative wear and delamination at 250–350 °C [44]. Moreover, the reported mechanism did not determine the direction of the temperature effect on wear: oxidative wear accompanied both increasing [27] and decreasing [37] specific wear rates. A classification of the 32 points with a stated dominant mechanism, using test temperature, normal load, counterface, contact geometry, manufacturing method and alloy as inputs, did not predict the mechanism of an omitted study better than always assigning the most frequent mechanism (16–34% versus 34% correct; Table S4). A sequence of regimes with fixed temperature boundaries can therefore not be derived from the available data; transition temperatures depend on the counterface, the contact conditions and the material, and Fig. 8 should be read as a compilation of reported observations rather than as a predictive map.

5. Conclusions

This review compiled dry sliding data of additively manufactured titanium alloys from 13 room-temperature and 20 elevated-temperature studies and compared them within each study. The main findings are:

5.1. Room-temperature behaviour

In the studies compared quantitatively, the specific wear rates ranged from about 0.4–16 $\times$ 10^{-4} $mm^3/(N{\cdot}m)$ and depended on the tribosystem at least as much as on the material. Room-temperature hardness did not consistently rank the wear resistance: in some studies the harder material wore less, as expected from Archard's relation, and in others it wore more.

5.2. Effect of temperature

The specific wear rate did not follow a common temperature dependence. It increased most against SiC, an Fe-based superalloy and in pin-on-disc tests against steel, and decreased mainly against Al_2O_3.

5.3. Manufacturing method

In the paired comparisons in which AM and conventionally processed materials were tested under identical conditions, the specific wear rate of the AM material ranged from about 0.6–2.1 times that of the conventional material at room temperature and from about 0.8–1.6 times at elevated temperature, and no AM technique performed consistently better than the others. AM titanium alloys can therefore reach wear rates comparable to those of conventionally processed material, and in these studies the effect of the manufacturing method was smaller than the effects of temperature and counterface.

5.4. Friction

The coefficient of friction was mostly between 0.2 and 0.6 and appeared to depend mainly on the counterface and the contact configuration. Where different manufacturing methods were tested under identical conditions, their coefficients of friction mostly differed by 0.05 or less. The coefficient of friction did not change in parallel with the wear rate, so a low coefficient of friction does not indicate low wear.

5.5. Test conditions

Increasing the normal load raised the specific wear rate in the pin-on-disc study but mostly lowered it in ball-on-flat tests, and this effect changed with temperature. In the only study that varied the sliding time, it changed the absolute wear rates but not the ranking of the test temperatures. Absolute values from different studies should therefore not be compared directly.

5.6. Tribo-layers

TiO_2 was found in all tribo-layers analysed by phase analysis, together with iron oxides transferred from steel counterfaces, but most studies characterized the layers by EDS or SEM only. The presence of a tribo-layer did not consistently coincide with lower wear; decreases in wear with temperature were observed mainly at low contact pressures. Hot hardness data of the tested materials were not available, and the only hot-strength data agreed qualitatively with Archard's relation if hardness is assumed to scale with strength.

5.7. Wear mechanisms

About half of the points were described by several mechanisms without ranking. Where the authors stated a dominant mechanism, it was mostly abrasive at room temperature, and oxidative wear became dominant between 150 and 550 °C in four studies; adhesive wear was named mainly against steel counterfaces. Because the counterface changed the reported mechanism even for the same material, and the test conditions did not predict the stated dominant mechanism, no wear regimes with fixed temperature boundaries could be derived.

6. Future outlook

The analysis identified the following needs for future studies:

6.1. Reporting of test conditions

Several studies did not report the sliding speed, sliding distance, track radius or ball diameter, and some reported wear only as wear depth or mass loss. Reporting the specific wear rate together with the contact geometry, initial Hertzian pressure, sliding distance and duration, and test environment would allow results to be compared between studies and is a prerequisite for data-driven models, which could not be established with the present dataset.

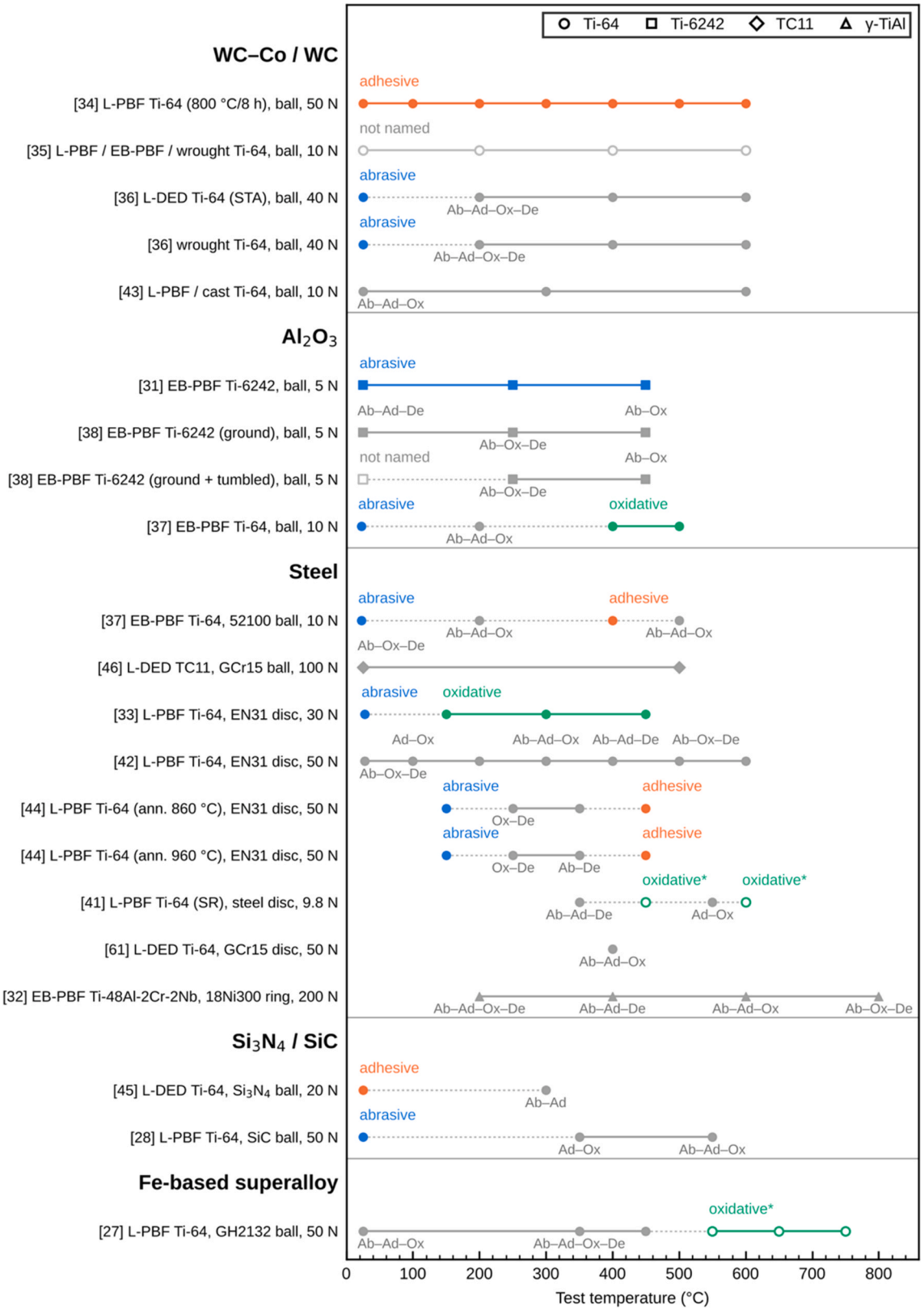


Fig. 8. Wear mechanisms reported by the authors at each test temperature, grouped by counterface material. Coloured symbols and labels denote a mechanism that the authors explicitly identified as dominant (blue: abrasive; orange: adhesive; green: oxidative). Grey symbols denote points at which no dominant mechanism was stated (mixed); their grey labels give the mechanisms named by the authors in a fixed order that does not imply a ranking (e.g., Ab–Ad–Ox; Ab: abrasive, Ad: adhesive, Ox: oxidative, De: delamination/fatigue) and are repeated only where the named mechanisms change. Open grey symbols denote that no mechanism was named. Solid lines connect temperatures with the same classification, and dotted lines indicate a change. Open green symbols with an asterisk denote oxidative wear for which the tribo-layer was documented by EDS or SEM only (Table 4). Marker shape indicates the alloy. Not shown: [39] (Section 2.4), tests in high vacuum [40] and small-amplitude tests [18]. Ti-64 = Ti-6Al-4V.

6.2. Characterization of tribo-layers

Most tribo-layers were characterized by EDS or SEM only. Phase identification on the worn surface and in the debris (XRD, Raman spectroscopy, TEM) and measurements of layer thickness and continuity are needed to relate tribo-layers to the measured wear.

6.3. Hot hardness and strength

None of the included studies measured the hot hardness of the tested materials. Hot hardness or hot strength data would allow Archard-type relations and the load-bearing capacity of tribo-layers to be evaluated at the test temperature.

6.4. Systematic test programmes

Fifteen of the 20 elevated-temperature studies investigated Ti-6Al-4V, alloys were compared within the same study only at room temperature, and elevated-temperature data for WAAM material are limited to one study with small-amplitude tests. Load and temperature were varied together in only four studies, and AM and conventionally processed materials were compared at elevated temperature in only three studies, all against WC–Co or WC counterfaces. Load–temperature test matrices with the same tribosystem, and comparisons of manufacturing methods against several counterfaces, would clarify the interactions identified in this review.

6.5. Service-relevant conditions

The included studies were isothermal dry sliding tests of limited duration. Components such as compressor parts and actuators are exposed to thermal cycling, fretting and long service times; tests under such conditions, combined with modelling, are needed for life prediction.

CRediT authorship contribution statement

Mehmet Can Katmer: Writing – original draft, Methodology, Investigation, Data curation, Conceptualization. **Onur Cavusoglu:** Writing – original draft, Investigation, Formal analysis, Conceptualization. **Hakan Gürün:** Writing – review & editing, Supervision, Project administration. **Ömer Asal:** Conceptualization, Investigation, Writing – review & editing.

Declaration of Generative AI and AI-assisted technologies in the writing process

During the preparation of the revised manuscript, the authors used Claude (Anthropic) to assist with the extraction of data from the cited studies and their checking against the original publications, and with editing of the revised text. After using this tool, the authors reviewed and edited the content as needed and take full responsibility for the content of the published article.

Declaration of Competing Interest

The authors declare that they have no known competing financial interests or personal relationships that could have appeared to influence the work reported in this paper.

Acknowledgements

This research was supported by Gazi University Scientific Research Projects (BAP) Unit under Project Code FDK-2024–9874.

Appendix A. Supporting information

Supplementary data associated with this article can be found in the online version at doi:10.1016/j.mtcomm.2026.116582.

Data availability

The data compiled in this review are provided as supplementary material

References

[1] B. Dutta, F.H. Froes, Additive manufacturing of titanium alloys: State of the art, challenges and opportunities, Butterworth-Heinemann, 2016.
[2] M.-T. Nguyen, V.-T. Trinh, Heat treatment for microstructure stabilizing of biomedical Ti-6Al-4V alloy fabricated by selective laser melting, MM Sci. J. 2024 (2024) 7453–7457, https://doi.org/10.17973/MMSJ.2024_10_2024060.
[3] Z. Liu, B. He, T. Lyu, Y. Zou, A review on additive manufacturing of titanium alloys for aerospace applications: Directed energy deposition and beyond Ti-6Al-4V, JOM 73 (2021) 1804–1818, https://doi.org/10.1007/s11837-021-04670-6.
[4] L.-C. Zhang, H. Attar, M. Calin, J. Eckert, Review on manufacture by selective laser melting and properties of titanium based materials for biomedical applications, Mater. Technol. 31 (2016) 66–76, https://doi.org/10.1179/1753555715Y.0000000076.
[5] T.S. Tshephe, S.O. Akinwamide, E. Olevsky, P.A. Olubambi, Additive manufacturing of titanium-based alloys- a review of methods, properties, challenges, and prospects, Heliyon 8 (2022) e09041, https://doi.org/10.1016/j.heliyon.2022.e09041.
[6] J. Tong, C.R. Bowen, J. Persson, A. Plummer, Mechanical properties of titanium-based Ti–6Al–4V alloys manufactured by powder bed additive manufacture, Mater. Sci. Technol. 33 (2017) 138–148, https://doi.org/10.1080/02670836.2016.1172787.
[7] Z. Wei, S. Attarilar, M. Ebrahimi, J. Li, Corrosion and wear behavior of additively manufactured metallic parts in biomedical applications, Metals 14 (2024) 96, https://doi.org/10.3390/met14010096.
[8] W. Zhang, J. Xu, Advanced lightweight materials for automobiles: a review, Mater. Des. 221 (2022) 110994, https://doi.org/10.1016/j.matdes.2022.110994.
[9] K. Takahashi, K. Mori, H. Takebe, Application of titanium and its alloys for automobile parts, MATEC Web Conf. 321 (2020) 02003, https://doi.org/10.1051/matecconf/202032102003.
[10] A.M. Nayeem, M.M.N. Hossain, Usage of additive manufacturing in the automotive industry: a review, Bangladesh J. Multidiscip. Sci. Res. 8 (2023) 9–20, https://doi.org/10.46281/bjmsr.v8i1.2135.
[11] C.Y. Yap, C.K. Chua, Z.L. Dong, Z.H. Liu, D.Q. Zhang, L.E. Loh, S.L. Sing, Review of selective laser melting: materials and applications, Appl. Phys. Rev. 2 (2015) 041101, https://doi.org/10.1063/1.4935926.
[12] J. Fiocchi, C.A. Biffi, D. Scaccabarozzi, B. Saggin, A. Tuissi, Enhancement of the damping behavior of Ti6Al4V alloy through the use of trabecular structure produced by selective laser melting, Adv. Eng. Mater. 22 (2020) 1900722, https://doi.org/10.1002/adem.201900722.
[13] T. DebRoy, H.L. Wei, J.S. Zuback, T. Mukherjee, J.W. Elmer, J.O. Milewski, A. M. Beese, A. Wilson-Heid, A. De, W. Zhang, Additive manufacturing of metallic components – process, structure and properties, Prog. Mater. Sci. 92 (2018) 112–224, https://doi.org/10.1016/j.pmatsci.2017.10.001.
[14] W.E. Frazier, Metal additive manufacturing: a review, J. Mater. Eng. Perform. 23 (2014) 1917–1928, https://doi.org/10.1007/s11665-014-0958-z.
[15] N. Zakerin, K. Morshed-Behbahani, D.P. Bishop, A. Nasiri, Review of tribological and wear behavior of alloys fabricated via directed energy deposition additive manufacturing, J. Manuf. Mater. Process. 9 (2025) 194, https://doi.org/10.3390/jmmp9060194.
[16] D. Svetlizky, M. Das, B. Zheng, A.L. Vyatskikh, S. Bose, A. Bandyopadhyay, J. M. Schoenung, E.J. Lavernia, N. Eliaz, Directed energy deposition (DED) additive manufacturing: physical characteristics, defects, challenges and applications, Mater. Today 49 (2021) 271–295, https://doi.org/10.1016/j.mattod.2021.03.020.
[17] H. Kaundal, R.K.R. Singh, T.K. Bera, Influence of process parameters on wear properties of wire arc additive manufactured Ti-6Al-4V alloy, J. Mater. Eng. Perform. 35 (2026) 21054–21065, https://doi.org/10.1007/s11665-026-13164-y.
[18] B. Guo, Y. Guo, D. Tian, Y. Han, X. Zhang, H. Bai, L. Xin, Unveiling the temperature effect on reciprocating sliding wear mechanism of a TA15 alloy fabricated by wire-arc additive manufacturing, Wear 562-563 (2025) 205655, https://doi.org/10.1016/j.wear.2024.205655.
[19] R. Shah, N. Pai, A. Rosenkranz, K. Shirvani, M. Marian, Tribological behavior of additively manufactured metal components, J. Manuf. Mater. Process. 6 (2022) 138, https://doi.org/10.3390/jmmp6060138.
[20] B. Vrancken, L. Thijs, J.-P. Kruth, J. Van Humbeeck, Heat treatment of Ti6Al4V produced by selective laser melting: microstructure and mechanical properties, J. Alloy. Compd. 541 (2012) 177–185, https://doi.org/10.1016/j.jallcom.2012.07.022.
[21] L. Facchini, E. Magalini, P. Robotti, A. Molinari, S. Höges, K. Wissenbach, Ductility of a Ti-6Al-4V alloy produced by selective laser melting of prealloyed powders, Rapid Prototyp. J. 16 (2010) 450–459, https://doi.org/10.1108/13552541011083371.

[22] S. Liu, Y.C. Shin, Additive manufacturing of Ti6Al4V alloy: a review, Mater. Des. 164 (2019) 107552, https://doi.org/10.1016/j.matdes.2018.107552.
[23] L.E. Murr, S.A. Quinones, S.M. Gaytan, M.I. Lopez, A. Rodela, E.Y. Martinez, D. H. Hernandez, E. Martinez, F. Medina, R.B. Wicker, Microstructure and mechanical behavior of Ti–6Al–4V produced by rapid-layer manufacturing, for biomedical applications, J. Mech. Behav. Biomed. Mater. 2 (2009) 20–32, https://doi.org/10.1016/j.jmbbm.2008.05.004.
[24] J.F. Archard, Contact and rubbing of flat surfaces, J. Appl. Phys. 24 (1953) 981–988, https://doi.org/10.1063/1.1721448.
[25] M.S. Bin Abdullah, M. Ramulu, The tribological behavior of electron beam powder bed fused Ti-6Al-4V: a review, Metals 15 (2025) 1170, https://doi.org/10.3390/met15111170.
[26] X. Jiang, J. Lu, N. Zhao, Z. Chen, Z. Zhao, A review of wear in additive manufacturing: wear mechanism, materials, and process, Lubricants 12 (2024) 321, https://doi.org/10.3390/lubricants12090321.
[27] R. Xu, Y. Zhu, J. Wu, P. Huang, M. Wu, W. Wang, C. Zhang, H. Yang, Hybrid high-temperature wear mechanisms of additive manufactured Ti-6Al-4V alloy, Tribol. Int. 205 (2025) 110559, https://doi.org/10.1016/j.triboint.2025.110559.
[28] J. Wu, R. Xu, Y. Duan, H. Lin, Y. Wu, Y. Zhu, L. Wang, Y. Zhu, B. Xu, J. Zhang, C. Zhang, Competitive effects between surface oxidation and softening behaviors on high-temperature wear evolution mechanisms of additive manufactured Ti-6Al-4V, Tribol. Int. 225 (2027) 112419, https://doi.org/10.1016/j.triboint.2026.112419.
[29] A. Molinari, G. Straffelini, B. Tesi, T. Bacci, Dry sliding wear mechanisms of the Ti6Al4V alloy, Wear 208 (1997) 105–112, https://doi.org/10.1016/S0043-1648(96)07454-6.
[30] P. Renner, S. Jha, Y. Chen, A. Raut, S.G. Mehta, H. Liang, A review on corrosion and wear of additively manufactured alloys, J. Tribol. 143 (2021) 050802, https://doi.org/10.1115/1.4050503.
[31] F. Davoodi, M. Taghian, P. Moazzen, M. Galati, M. Mohammadi, A. Saboori, Microstructural anisotropy and near-isotropic tribological behavior of electron beam powder bed fusion Ti-6Al-2Sn-4Zr-2Mo alloy, Prog. Addit. Manuf. 11 (2026) 7075–7097, https://doi.org/10.1007/s40964-026-01717-5.
[32] J. Yan, Y. Xie, B. Ou, X. Meng, B. Cai, Y. Zhang, S. Fang, Process optimization and tribological behavior of Ti-48Al-2Cr-2Nb prepared by selective electron beam melting, Eng. Fail. Anal. 165 (2024) 108837, https://doi.org/10.1016/j.engfailanal.2024.108837.
[33] K. Praveenkumar, J. Vishnu, C. Samuel S, V. Gopal, M. Arivarasu, J.M. Lackner, B. Meier, D. Karthik, S. Suwas, S. Swaroop, K.G. Prashanth, M.K. Yadav, G. Manivasagam, High temperature dry sliding wear behaviour of selective laser melted Ti-6Al-4V alloy surfaces, J. Mater. Process. Technol. 329 (2024) 118439, https://doi.org/10.1016/j.jmatprotec.2024.118439.
[34] X. Liang, P. Du, S. Li, C. Zhang, Tribological properties of additive manufactured Ti6Al4V against cemented carbide under dry sliding conditions, Tribol. Int. 167 (2022) 107358, https://doi.org/10.1016/j.triboint.2021.107358.
[35] H. Li, Z.W. Chen, M. Ramezani, Effect of temperature on sliding wear behavior of Ti-6Al-4V alloy processed by powder bed fusion additive manufacturing techniques, J. Mater. Eng. Perform. 31 (2022) 8940–8954, https://doi.org/10.1007/s11665-022-06959-2.
[36] Z. Zhang, Z. Li, S. Pan, X. Chai, Enhanced strength and high-temperature wear resistance of Ti6Al4V alloy fabricated by laser solid forming, J. Manuf. Sci. Eng. 144 (2022) 111011, https://doi.org/10.1115/1.4054901.
[37] S. Alvi, M. Neikter, M.-L. Antti, F. Akhtar, Tribological performance of Ti6Al4V at elevated temperatures fabricated by electron beam powder bed fusion, Tribol. Int. 153 (2021) 106658, https://doi.org/10.1016/j.triboint.2020.106658.
[38] F. Davoodi, P. Moazzen, M. Taghian, M. Galati, M. Mohammadi, A. Saboori, Synergistic surface engineering of PBF-EB/M Ti-6Al-2Sn-4Zr-2Mo: linking support-fingerprint morphology to high-temperature tribological behavior, Prog. Addit. Manuf. 11 (2026) 5935–5954, https://doi.org/10.1007/s40964-026-01677-w.
[39] Y. Liu, C. Li, Y. Yang, Y. Sun, W. Zhang, X. Zhang, The effect of temperature rise on the wear mechanisms of 3D-printed TC4 alloy under different loads and ambient temperatures, Mater. Charact. 231 (2026) 115885, https://doi.org/10.1016/j.matchar.2025.115885.
[40] M.M. Basha, M.R. Sankar, T.S.R.Ch. Murthy, S. Majumdar, High-temperature tribology of selective laser-melted titanium alloys: role of adhesive wear, J. Tribol. 146 (2024) 061701, https://doi.org/10.1115/1.4064540.
[41] M.C. Kittur, D.M. Goudar, T. Jagadeesha, K. Raju, R.V. Kurahatti, S.K. Bhat, Microstructure, thermal, and wear properties of selective laser melted Ti-6Al-4V at high temperatures, J. Mater. Eng. Perform. (2026), https://doi.org/10.1007/s11665-026-15040-1.
[42] J. Joshy, B. Kuriachen, Investigations in to the wear behavior of additively manufactured Ti6Al4V at elevated temperatures, Wear 571 (2025) 205774, https://doi.org/10.1016/j.wear.2025.205774.
[43] A. Çakar, K. Kılıçay, Comparison of high-temperature friction and wear behaviours of Ti6Al4V produced by additive manufacturing and casting, Proc. Inst. Mech. Eng. B J. Eng. Manuf. 239 (2025) 1218–1227, https://doi.org/10.1177/09544054241272895.
[44] D. Amrishraj, M. Natesh, T. Senthilvelan, B. Nethravathi, P. Anagolkar, T. Ramprabhu, Studies on high temperature wear behavior of additively manufactured Ti-6Al-4V alloy using machine learning models, J. Mater. Eng. Perform. 35 (2026) 13903–13919, https://doi.org/10.1007/s11665-025-12596-2.
[45] Z. Tai, Y. Wei, V. Trofimov, D. Wang, G. Bi, Friction and wear behavior of TiN/Ti6Al4V composite material synthesized in-situ using laser directed energy deposition, Sci. Rep. 16 (2026) 26435, https://doi.org/10.1038/s41598-026-56859-x.
[46] C. Chen, D. Liu, X. Fan, K. Guo, Q. Geng, L. Li, J. Ju, J. Wang, R. Navio Gilaberte, Y. Liu, Z. Zhang, B. Sun, H. Chen, Wear resistance enhancement in titanium matrix composites via in-situ synthesized TiBw by laser melting deposition, Tribol. Int. 226 (2027) 112648, https://doi.org/10.1016/j.triboint.2026.112648.
[47] M. Hemachandra, S. Thapliyal, K. Adepu, A review on microstructural and tribological performance of additively manufactured parts, J. Mater. Sci. 57 (2022) 17139–17161, https://doi.org/10.1007/s10853-022-07736-1.
[48] M.J. Page, J.E. McKenzie, P.M. Bossuyt, I. Boutron, T.C. Hoffmann, C.D. Mulrow, L. Shamseer, J.M. Tetzlaff, E.A. Akl, S.E. Brennan, et al., The PRISMA 2020 statement: an updated guideline for reporting systematic reviews, BMJ 372 (2021) n71, https://doi.org/10.1136/bmj.n71.
[49] N. Kang, M. El Mansori, E. Feng, C. Zhao, Y. Zhao, X. Lin, Sliding wear and induced-microstructure of Ti-6Al-4V alloys: effect of additive laser technology, Tribol. Int. 173 (2022) 107633, https://doi.org/10.1016/j.triboint.2022.107633.
[50] H. Li, M. Ramezani, Z.W. Chen, Dry sliding wear performance and behaviour of powder bed fusion processed Ti-6Al-4V alloy, Wear 440-441 (2019) 203103, https://doi.org/10.1016/j.wear.2019.203103.
[51] H. Attar, M.J. Bermingham, S. Ehtemam-Haghighi, A. Dehghan-Manshadi, D. Kent, M.S. Dargusch, Evaluation of the mechanical and wear properties of titanium produced by three different additive manufacturing methods for biomedical application, Mater. Sci. Eng. A 760 (2019) 339–345, https://doi.org/10.1016/j.msea.2019.06.024.
[52] J. Huang, W. Zhang, W. Fang, Y. Yi, Tribology properties of additively manufactured Ti6Al4V alloy after heat treatment, Tribol. Int. 185 (2023) 108485, https://doi.org/10.1016/j.triboint.2023.108485.
[53] M.M. Basha, T.S.R.Ch Murthy, B. Paul, A.K. Sahu, M.R. Sankar, Experimental investigation on dry sliding wear characteristics of additive manufactured titanium alloy features with various carbide balls, Tribol. Int. 213 (2026) 111029, https://doi.org/10.1016/j.triboint.2025.111029.
[54] X. Luo, Y. Li, C. Yang, C. Zhao, H. Ma, T. Song, M. Sun, X. Liu, D. Li, N. Li, Insights into laser powder bed fused β-type titanium alloy: investigating corrosion behavior and wear properties after post-heat treatment, J. Mater. Res. Technol. 37 (2025) 1596–1605, https://doi.org/10.1016/j.jmrt.2025.06.120.
[55] H. Attar, K.G. Prashanth, A.K. Chaubey, M. Calin, L.C. Zhang, S. Scudino, J. Eckert, Comparison of wear properties of commercially pure titanium prepared by selective laser melting and casting processes, Mater. Lett. 142 (2015) 38–41, https://doi.org/10.1016/j.matlet.2014.11.156.
[56] G.V. Krishna Pradeep, M. Duraiselvam, K. Siva Prasad, A. Mohammad, Tribological behavior of additive manufactured γ-TiAl by electron beam melting, Trans. Indian. Inst. Met. 73 (2020) 1661–1667, https://doi.org/10.1007/s12666-020-01950-8.
[57] J. Joshy, B. Kuriachen, N. Ahmad, N. Shamsaei, S. Shao, Sliding wear behavior of additively manufactured Ti-6Al-4V: the effect of thermal treatment, Wear 580-581 (2025) 206249, https://doi.org/10.1016/j.wear.2025.206249.
[58] D. Sharma, M. Kamran, N.K. Paraye, R. Anant, Insights into the wear behaviour of electron beam melted Ti–6Al–4V alloy in the as-built and the heat-treated conditions, J. Manuf. Process. 71 (2021) 669–678, https://doi.org/10.1016/j.jmapro.2021.09.060.
[59] M. Naghyan Fesharaki, M. Atapour, S.M. Nahvi, M. Galati, A. Saboori, Tribological response and microstructure evolution of electron beam powder bed fusion additively manufactured Ti–6Al–2Sn–4Zr–2Mo alloy, Prog. Addit. Manuf. 11 (2026) 1139–1154, https://doi.org/10.1007/s40964-025-01402-z.
[60] D. Du, W. Zhang, J. An, Two types of wear mechanisms governing transition between mild and severe wear in Ti-6Al-4V alloy during dry sliding at temperatures of 20–250 °C, Materials 15 (2022) 1416, https://doi.org/10.3390/ma15041416.
[61] Y. Zheng, R. Xiong, Z. Zhao, C. Zhao, W. Liu, S. Wei, Microstructure and high-temperature wear/oxidation behaviors of TiN/TC4 composites in-situ fabricated by laser melting deposition in N2-containing atmosphere, Compos. Commun. 49 (2024) 101992, https://doi.org/10.1016/j.coco.2024.101992.
[62] K.L. Johnson, Contact Mechanics, Cambridge University Press, Cambridge, 1985, https://doi.org/10.1017/CBO9781139171731.
[63] J.F. Shackelford, Y.-H. Han, S. Kim, S.-H. Kwon (Eds.), CRC Materials Science and Engineering Handbook, 4th ed., CRC Press, Boca Raton, FL, 2015.
[64] S. Okamoto, Y. Nakazono, K. Otsuka, Y. Shimoitani, J. Takada, Mechanical properties of WC/Co cemented carbide with larger WC grain size, Mater. Charact. 55 (2005) 281–287, https://doi.org/10.1016/j.matchar.2005.06.001.
[65] Y. Qin, C. Zheng, H. Jin, S. Xu, J. Zhang, C. Wei, C. Zhang, X. Li, The effects of vacancies and fission products on the structures and properties of β-SiC: a first-principles study, J. Mater. Res. Technol. 24 (2023) 5598–5612, https://doi.org/10.1016/j.jmrt.2023.04.103.
[66] J.C. Colombo-Pulgarín, C.A. Biffi, M. Vedani, D. Celentano, A. Sánchez-Egea, A. D. Boccardo, J.-P. Ponthot, Beta titanium alloys processed by laser powder bed fusion: A review, J. Mater. Eng. Perform. 30 (2021) 6365–6388, https://doi.org/10.1007/s11665-021-05800-6.
[67] N. Kang, M.E. Mansori, N. Coniglio, C. Coddet, Nano-wear-induced behavior of selective laser melting commercial pure titanium, Procedia Manuf. 26 (2018) 1034–1040, https://doi.org/10.1016/j.promfg.2018.07.136.
[68] A. Akman, Tribocorrosion behaviour and surface modification of laser powder bed fusion (LPBF) processed β-type Ti-Nb alloys for implant applications. PhD Thesis, Technische Universität Dresden, Dresden, Germany, 2026.
[69] L. Zhou, X. Yang, J. Sun, J. Chen, C. Li, The anisotropy wear and tribocorrosion performances of pure titanium fabricated by laser powder bed fusion, Mater. Lett. 399 (2025) 139063, https://doi.org/10.1016/j.matlet.2025.139063.
[70] D. Gu, Y.-C. Hagedorn, W. Meiners, G. Meng, R.J.S. Batista, K. Wissenbach, R. Poprawe, Densification behavior, microstructure evolution, and wear

performance of selective laser melting processed commercially pure titanium, Acta Mater. 60 (2012) 3849–3860, https://doi.org/10.1016/j.actamat.2012.04.006.
[71] K. Yang, J. Wang, G.-Y. Yang, L. Jia, Improved mechanical and wear properties of Ti–35Nb–5Ta–7Zr–xSi alloys fabricated by selective electron beam melting for biomedical application, J. Cent. South. Univ. 29 (2022) 3825–3835, https://doi.org/10.1007/s11771-022-5203-6.
[72] H. Kovacı, Comparison of the microstructural, mechanical and wear properties of plasma oxidized Cp-Ti prepared by laser powder bed fusion additive manufacturing and forging processes, Surf. Coat. Technol. 374 (2019) 987–996, https://doi.org/10.1016/j.surfcoat.2019.06.095.
[73] K. Huang, F. Xu, X. Liu, S. Liu, Q. Wang, I. Baker, M. Song, H. Wu, Microstructure, mechanical, and tribological properties of Nb-doped TiAl alloys fabricated via laser metal deposition, Materials 17 (2024) 4260, https://doi.org/10.3390/ma17174260.
[74] A. Yin, W. Yu, W. Zhu, W. Li, V. Ji, C. Jiang, Microstructural characterization and wear performance of shot-peened TA15 titanium alloy fabricated by SLM, Mater. Charact. 209 (2024) 113747, https://doi.org/10.1016/j.matchar.2024.113747.
[75] S.S. Al-Bermani, M.L. Blackmore, W. Zhang, I. Todd, The origin of microstructural diversity, texture, and mechanical properties in electron beam melted Ti-6Al-4V, Metall. Mater. Trans. A 41 (2010) 3422–3434, https://doi.org/10.1007/s11661-010-0397-x.
[76] M. Jamil, M.I. Hussain, A.M. Khan, K.A. Al-Ghamdi, A comparative study on microstructural, mechanical and cryogenic machinability of Ti6Al4V fabricated via SLM and EBM additive manufacturing technologies, J. Mater. Res. Technol. 41 (2026) 3343–3358, https://doi.org/10.1016/j.jmrt.2026.01.185.
[77] L.R. Kanyane, A.P. Popoola, S. Pityana, M. Tlotleng, Heat-treatment effect on anti-corrosion behaviour and tribological properties of LENS in-situ synthesized titanium aluminide, Int. J. Lightweight Mater. Manuf. 5 (2022) 153–161, https://doi.org/10.1016/j.ijlmm.2021.11.006.
[78] M.N. Doğu, Z. Esen, K. Davut, E. Tan, B. Gümüş, A.F. Dericioglu, Microstructural and texture evolution during thermo-hydrogen processing of Ti6Al4V alloys produced by electron beam melting, Mater. Charact. 168 (2020) 110549, https://doi.org/10.1016/j.matchar.2020.110549.
[79] H. Tan, M. Guo, A.T. Clare, X. Lin, J. Chen, W. Huang, Microstructure and properties of Ti-6Al-4V fabricated by low-power pulsed laser directed energy deposition, J. Mater. Sci. Technol. 35 (2019) 2027–2037, https://doi.org/10.1016/j.jmst.2019.05.008.